https://doi.org/10.5194/egusphere-2022-1137
Preprint. Discussion started: 20 December 2022

Effects of a biased LAI data assimilation system on hydrological variables and carbon uptake over Europe

Samuel Scherrer[1,2], Gabriëlle De Lannoy[2], Zdenko Heyvaert[1,2], Michel Bechtold[2], Clement Albergel[3], Tarek S. El-Madany[4], and Wouter Dorigo[1]

[1]Department of Geodesy and Geoinformation, TU Wien, Vienna, Austria
[2]Department of Earth and Environmental Sciences, KU Leuven, Heverlee, Belgium
[3]European Space Agency Climate Office, ECSAT, Didcot, UK
[4]Max Planck Institute for Biogeochemistry, Department Biogeochemical Integration, Jena, Germany

Correspondence: Samuel Scherrer (samuel.scherrer@geo.tuwien.ac.at)

Abstract. Data assimilation (DA) of remotely sensed leaf area index (LAI) can help to improve land surface model estimates of energy, water, and carbon variables. So far, most studies have used bias-blind LAI DA approaches, i.e. without correcting for biases between model forecasts and observations. This might hamper the performance of the DA algorithms in the case of large biases in either observations or simulations, or both. We perform bias-blind and bias-aware DA of the Copernicus Global Land Service LAI into the Noah-MP land surface model forced by the ERA5 reanalysis over Europe in the 2002–2019 period, and evaluate how the choice of bias correction affects estimates of gross primary productivity (GPP), evapotranspiration (ET), runoff, and soil moisture.

In areas with a large LAI bias, the bias-blind LAI DA leads to a reduced bias between observed and modelled LAI, an improved agreement of GPP, ET, and runoff estimates with independent products, but a worse agreement of soil moisture estimates with the European Space Agency Climate Change Initiative (ESA CCI) soil moisture product. Bias-blind LAI DA can also lead to unrealistic shifts in soil moisture climatologies, for example when the assimilated LAI data in irrigated areas are much higher than those simulated without any irrigation activated. Furthermore, the bias-blind LAI DA produces a pronounced sawtooth pattern due to model drift between update steps. This model drift also propagates to short-term estimates of GPP and ET, and to internal DA diagnostics that indicate a suboptimal DA system performance.

The bias-aware approaches based on a priori rescaling of LAI observations to the model climatology avoid the negative effects of the bias-blind assimilation. They retain the improvements of GPP anomalies from the bias-blind DA, but forego improvements in the root mean square deviation (RMSD) of GPP, ET, and runoff. As an alternative to rescaling, we discuss the implications of our results for model calibration or joint parameter and state update DA, which has the potential to combine bias reduction with optimal DA system performance.

1 Introduction

Vegetation plays a major role in climatic interactions between the land surface and the atmosphere. Via transpiration and photosynthesis, it contributes to the exchange of energy, water, and carbon at the surface, and links the moisture in the deeper

https://doi.org/10.5194/egusphere-2022-1137
Preprint. Discussion started: 20 December 2022

soil layers to the atmosphere (Bonan, 2019). On short timescales, these exchanges can impact precipitation and atmospheric circulation (Betts et al., 1996; Miralles et al., 2016). On longer timescales, the net uptake of CO_2 by vegetation (Friedlingstein et al., 2022) might be decreased due to climate change, contributing to rising CO_2 levels (Green et al., 2019; Walker et al., 2021). Land surface models (LSMs) are often used to estimate these exchange fluxes as part of Earth system models or as land component in numerical weather prediction (NWP) systems (e.g., Balsamo et al., 2009; Lawrence et al., 2019; Skamarock et al., 2019). An accurate description of vegetation in LSMs can therefore improve estimates of evapotranspiration (ET) in NWP (Boussetta et al., 2013), or can be used to estimate how vegetation will develop under a changed climate (Laanaia et al., 2016) and how this affects the land carbon sink (Tharammal et al., 2019a, b; Green et al., 2019).

However, the dynamic simulation of vegetation in global LSMs is still in its infancy and has large uncertainties, especially in dry climates (Fox et al., 2018; Mahmud et al., 2021). Satellite-based vegetation data assimilation (DA) can be used to reduce the uncertainties of the vegetation-related LSM estimates. Satellite-derived leaf area index (LAI) is commonly used for DA, because it can be derived from optical sensors fairly accurately (Fang et al., 2019) and is also available as model state variable in several land surface models with a dynamic vegetation component. Satellite LAI has for example been assimilated into the *Interactions between Soil Biosphere Atmosphere* (ISBA) LSM (Sabater et al., 2008; Barbu et al., 2014; Fairbairn et al., 2017; Albergel et al., 2017; Mucia et al., 2020), the *Noah LSM with multiparameterisation options* (Noah-MP; e.g., Kumar et al., 2019b, 2021; Rahman et al., 2022; Nie et al., 2022), the *Community Land Model* (CLM; e.g., Fox et al., 2018; Ling et al., 2019), and the *Carbon-Tiled ECMWF Scheme for Surface Exchange over Land* (CTESSEL; e.g., Jarlan et al., 2008). Alternatives are, for example, to use microwave brightness temperatures to simultaneously update soil moisture and LAI (Sawada and Koike, 2014; Sawada et al., 2015) or to use microwave vegetation optical depth (VOD) retrievals to update LAI (Kumar et al., 2020, 2021).

The most commonly used methods for assimilating LAI into LSMs are based on the Kalman filter. A fundamental assumption of these methods is that modelled LAI and observed LAI are unbiased. Yet, in reality, biases nearly always exist. This includes biases of both model estimates and observations with respect to the unknown true value, and between the model estimates and observations themselves. If the observations are closer to the true value than the model estimates, a “bias-blind” DA (Dee, 2005) is able to correct the model bias to some extent, because it pulls the model closer towards the observations and, hence, the true values. This comes at the risk of introducing unintended negative side effects. For example, it is possible that other processes (e.g., transpiration) are only represented well for a biased model climatology. Large updates in a subset of the model state might therefore propagate to other model components, which can negatively affect estimates of state variables and fluxes of these processes (De Lannoy et al., 2007b; Crow et al., 2020). Furthermore, if the model equilibrium state is far away from the observations, the updates towards the observations might not persist for long. Instead, the model drifts back towards its original state, leading to a sawtooth-like pattern in the resulting time series and potentially also to unrealistic water, carbon and energy flux estimates (Dee, 2005; De Lannoy et al., 2007b). Changes in observation frequency or periodically missing data may then also introduce spurious trends in the analysis (Dee, 2005).

Most LAI assimilation studies so far used bias-blind approaches, i.e. they did not apply any bias correction methods to account for existing biases between modelled LAI and observed LAI. This is often justified by the argument that the bias is caused by model deficiencies (e.g., Fairbairn et al., 2017; Fox et al., 2018; Albergel et al., 2020). Nonetheless, there are indications that the presence of bias affects the performance of LAI assimilation. Albergel et al. (2017) and Albergel et al. (2020) noticed systematic drifts towards the previous model estimate on days without observations. Kumar et al. (2019b); Mocko et al. (2021) also found model drifts leading to sawtooth patterns in the analysed LAI when using the Noah-MP LSM with dynamic vegetation.

Various techniques have been used to limit the negative effects listed above. Albergel et al. (2017, 2020) and Mucia et al. (2021) additionally assimilated surface soil moisture retrievals. This additional constraint can help to prevent negative side-effects of the LAI DA on the model hydrology, but only in regions and periods where sufficient soil moisture observations are available. Kumar et al. (2019b); Mocko et al. (2021) and Rahman et al. (2022) interpolated their assimilated LAI product to daily values to prevent issues due to different observation frequencies and to limit the drift towards the original equilibrium state. Fox et al. (2018) adaptively inflated the model error in case of large bias between modelled LAI and the observations. The latter two techniques force the analysis to stay close to the observations, which begs the question of whether it might be more suitable to use a direct insertion approach or to prescribe the observed LAI instead of modelling it dynamically, as for example done by Huang et al. (2022).

Bias-aware data assimilation is another possible avenue to handle bias between models and observations. This includes a priori rescaling approaches, which map the observations into the model space based on a priori estimates of model and observation statistics (e.g., Reichle and Koster, 2004; Jarlan et al., 2008; Khaki et al., 2020), or online approaches which adaptively estimate dynamic bias corrections (e.g., Derber and Wu, 1998; Dee, 2005; De Lannoy et al., 2007a). Only a few studies considered bias-aware approaches based on rescaling for LAI DA (Jarlan et al., 2008; Khaki et al., 2020). However, no study so far directly compared bias-blind and bias-aware LAI DA.

In this article, we compare the bias-blind LAI DA with bias-aware LAI DA using two a priori rescaling techniques commonly used for satellite DA. More specifically, we assimilate Copernicus Global Land Service (CGLS) LAI (Smets et al., 2019) into the Noah-MP model (Niu et al., 2011) forced with the fifth-generation European Center for Medium-Range Weather Forecasts (ECMWF) Reanalysis (ERA5; Hersbach et al., 2020) reanalysis over Europe, and quantify the effect of bias-blind and bias-aware DA on vegetation and surface water flux and state estimates.

A detailed description of the used model, data, and rescaling approaches can be found in section 2. Section 3 shows the impacts of the bias-blind DA on the vegetation and hydrology model estimates, evaluates the results using independent reference datasets, and compares the model simulations to in situ data from Majadas, Spain. Additionally, we provide an analysis of the sawtooth pattern in the bias-blind DA and of internal DA diagnostics. We discuss the implications of our results for LAI DA design and model calibration in section 4. A summary of our main conclusions is given in section 5.

https://doi.org/10.5194/egusphere-2022-1137
Preprint. Discussion started: 20 December 2022

2 Data & Methods

2.1 Land surface model

We used the Noah-MP LSM (Niu et al., 2011; Yang et al., 2011) version 4.0.1 with dynamic vegetation as implemented in the NASA Land Information System (LIS; Kumar et al., 2006; Peters-Lidard et al., 2007)). The Noah-MP LSM is based on the Noah LSM, which is widely used for land surface modelling and DA on a regional to global scale (e.g., Rodell et al., 2004; Kumar et al., 2014, 2019a; Maertens et al., 2021). Noah-MP includes a multitude of optional improvements for snow, water, and vegetation modelling. It has already been used to update LAI using optical satellite imagery (Kumar et al., 2019b; Erlingis et al., 2021; Rahman et al., 2022) and microwave vegetation optical depth (Kumar et al., 2020, 2021).

The dynamic vegetation model of Noah-MP is based on the vegetation model in the Biosphere–Atmosphere Transfer Scheme (BATS) model (Dickinson et al., 1998). In this model, gross primary production (GPP) is allocated to the four vegetation carbon pools (leaves, non-woody stems, wood, and fine roots) in each simulation step. LAI is calculated from leaf carbon mass by multiplying with a vegetation type dependent specific leaf area. It can feed back to other model state variables and fluxes via its effect on photosynthesis, evapotranspiration (ET), precipitation interception, and runoff. Changes in LAI can therefore also induce changes in the model hydrology.

Maps of soil texture and land cover, and multiple parameters based on these, are required as input to the model and were taken from the NCCS Dataportal (https://portal.nccs.nasa.gov/lisdata_pub/data/PARAMETERS/; Tian et al., 2008). We used the STATSGO-FAO (*State Soil Geography - Food Agricultural Organisation*) soil texture map produced by the *National Center for Atmospheric Research* (NCAR). For vegetation, we used the IGBP-NCEP (*International Geosphere-Biosphere Programme - National Centers for Environmental Prediction*) land cover map based on Friedl et al. (2002). This map classifies some pixels in France, Spain, Ireland and Germany as evergreen broadleaf forests, which the model interprets as tropical rainforests. We therefore replaced these pixels with the land cover class in the University of Maryland (UMD) land cover map (Hansen et al., 2000).

As forcing, Noah-MP requires the lowest level atmospheric model (about 10 m above ground level) air temperature, wind speed, specific humidity and pressure, the downwelling fluxes of shortwave and longwave radiations, as well as precipitation (partitioned into solid and liquid phases). We used data from ERA5, the latest ECMWF reanalysis, for this purpose. The initial model state was obtained from a 30-year deterministic spinup run, cycling 3 times with the forcing data from 2000 to 2010, followed by 2 years of ensemble spinup from 2000 to 2002.

The model domain in this study covers Europe, as well as parts of Northern Africa and the Middle East on a regular grid at a 0.25° resolution (ranging from 29.875°N, −11.375°E to 71.625°N, 40.125°E). It includes a wide range of climates and vegetation types, from tundra and boreal forests in Scandinavia to the Sahara Desert. We performed the model simulations from 2002 through 2019, using a 15-minute simulation time step and outputting daily averages centred at 0:00 UTC.

https://doi.org/10.5194/egusphere-2022-1137
Preprint. Discussion started: 20 December 2022

2.2 LAI observations

We assimilated the Copernicus Global Land Service (CGLS) satellite LAI product derived from *Project for On-Board Autonomy - Vegetation* (PROBA-V) and *Satellite Pour l'Observation de la Terre - Vegetation* (SPOT-VGT) (Verger et al., 2014). This product has been used for LAI DA before, e.g. by Barbu et al. (2014), Albergel et al. (2017), and Mucia et al. (2020). The 1 km resolution CGLS LAI product is provided as 10-daily images composed from an adaptive window of 15 to 60 days, depending on the availability of valid measurements (Smets et al., 2019). We masked out gap-filled values and upscaled the data to 0.25° resolution by averaging over all observations within one model grid cell. In contrast to Kumar et al. (2019b), we did not interpolate the LAI to daily values, but we assimilated the aggregated data every 10 days at 0:00 UTC, where and when they are available.

2.3 Data assimilation

We used a one-dimensional ensemble Kalman Filter (EnKF; Evensen, 2003) for assimilating the CGLS LAI observations into the Noah-MP LSM. The EnKF is a two-step procedure. First, the model simulates the land surface state $x^f(t)$ at the next assimilation time step (forecast). Then, the model state is updated to agree better with the observations $y(t)$, resulting in the analysis $x^a(t)$. The magnitude of the update (increment) depends on the innovations (observation minus forecast) and the relative sizes of the forecast and observation error variances. In a properly configured DA system, the normalised innovations (innovations divided by total error standard deviation) should be temporally uncorrelated and follow a standard normal distribution, i.e., the innovation sequence should be a white noise sequence with zero mean and unit standard deviation (Desroziers et al., 2005).

In the EnKF, the forecast error is estimated based on an ensemble of model simulations. We used 24 ensemble members, one of which was driven by the original forcing data, while the others were driven by perturbed radiation and precipitation forcing data. Additionally, we applied normally distributed perturbations to the model LAI state variable with a mean of zero and a standard deviation of 0.01 $\mathrm{m^2 m^{-2}}$ every 3 hours for the 23 perturbed ensemble members. The unperturbed ensemble member was used to correct for perturbation biases due to nonlinear processes using the method described by Ryu et al. (2009). All of the perturbation specifications and the observation error standard deviation of 0.05 $\mathrm{m^2 m^{-2}}$ were set following Kumar et al. (2019b).

To remove systematic differences between the modelled and observed LAI, we implemented two a priori rescaling methods: climatological cumulative distribution function (CDF) matching and a seasonal rescaling of the first and second moments. CDF-matching is commonly used for soil moisture DA without distinguishing the various seasons (e.g., Reichle and Koster, 2004; Drusch et al., 2005; Draper et al., 2012; Parrens et al., 2014; Barbu et al., 2014). It attempts to correct the biases in all statistical moments by non-linearly transforming the observation data such that the empirical CDF of the rescaled LAI data matches the empirical CDF of the modelled data. To estimate the empirical CDFs for each grid cell individually in a robust way, we opted to bin the data between the 2^{nd} and 98^{th} percentile. We then estimated the CDF by linearly interpolating the percentile values between the bin edges. For values outside the [2, 98] interval, the lines for the first and last bin are extrapolated to 0 and 100, respectively. The resulting curve is discretised into 100 equally spaced bins over the full data range for use in the

https://doi.org/10.5194/egusphere-2022-1137
Preprint. Discussion started: 20 December 2022

numerical rescaling procedure. When using the CDF-matching for rescaling, the observation error standard deviations are also rescaled for each grid cell individually by multiplying with the ratio of the modelled and observed LAI standard deviations.

The seasonal rescaling is an adaption of the additive seasonal mean correction scheme commonly used for brightness temperature DA (De Lannoy and Reichle, 2016; Lievens et al., 2017; Girotto et al., 2019; Bechtold et al., 2020). Similar to LAI, brightness temperatures also have a strong seasonal component. The additive rescaling only corrects biases in the first moment (mean). This is valid if the difference in anomaly variance between the model and observations is related to different error levels, i.e., the signal variances are similar (Yilmaz and Crow, 2013). In our case, differences in anomaly variance are strongly driven by differences in the dynamic range of observations and model estimates. We assume that the differences in the dynamic range also result in differences in error levels, and therefore additionally corrected for the standard deviation of model and observation.

For the seasonal rescaling, we calculated the rescaled observation values LAI_o' at each time t via

$$LAI_o'(t) = \mu_m(doy(t)) + \frac{\sigma_m}{\sigma_o} \cdot (LAI_o(t) - \mu_o(doy(t))),$$

with $\mu_\star(doy(t))$ the mean modelled (m) or observed (o) LAI value for the given day of year, and $\sigma_\star$ the standard deviation of the modelled or observed LAI time series at individual grid cells. The latter is mainly indicative of the magnitude of the seasonal variations. The mean seasonal cycle of modelled and observed LAI was estimated through a three-step procedure as implemented in the python package *pytesmo* (Paulik et al., 2022), i.e. (i) apply a smoothing with a 5-day moving window (ii) average values over days of year across multiple years (doy), and (iii) smooth the obtained seasonal cycle using a window of 31 days. When using the seasonal rescaling we also rescale the observation error standard deviation for each grid cell individually by multiplying with σ_m/σ_o.

We performed four model runs in total, one open loop run (OL) without any data assimilation (but applying the same perturbations), and one bias-blind and two bias-aware LAI DA runs:

- no bias correction (*bias-blind*)
- CDF matching for bias correction (*CDF-matched*)
- seasonal bias correction (*seasonally scaled*)

2.4 Evaluation metrics

To evaluate the performance of the OL and DA simulations, we calculated the root mean square deviation (RMSD), linear correlation (R) and linear anomaly correlation (R_{anom}) with independent reference datasets.

RMSD is a common measure for the overall disagreement between two datasets. It consists of a bias component due to bias in the first and second moments (mean and variance bias), and a correlation component due to disagreement of the temporal patterns (Gruber et al., 2020). When applied to time series with a strong seasonal cycle, as is the case for most variables we evaluate, it is dominated by mean bias and bias in the representation of the seasonal cycle. It is therefore mainly indicative of systematic disagreement between modelled and reference data.

https://doi.org/10.5194/egusphere-2022-1137
Preprint. Discussion started: 20 December 2022

Linear correlation R is not affected by mean or variance bias, but in the case of strong seasonal cycle, it is also dominated by bias in the representation of the seasonal cycle. It therefore quantifies how well the shapes of the seasonal cycles (e.g., peak location, phase shift) of two datasets match.

For assessing the agreement in the intra- and inter-annual temporal variations, we used linear anomaly correlation (R_{anom}). The anomalies are calculated by subtracting the long-term mean seasonal cycle for the 2003–2019 period from the original data for each grid cell. The mean seasonal cycle is calculated the same way as the seasonal cycle used for the seasonal observation rescaling (see subsection 2.3).

To make the metric improvements comparable over different variables and metrics we calculated the normalised information contributions (NIC; Kumar et al., 2009, 2014) for the three metrics:

$$NIC\ RMSD = \frac{RMSD_{OL} - RMSD_{DA}}{RMSD_{OL}}$$

$$NIC\ R = \frac{R_{DA} - R_{OL}}{1 - R_{OL}}$$

$$NIC\ R_{anom} = \frac{R_{anom,DA} - R_{anom,OL}}{1 - R_{anom,OL}}.$$

Positive NIC values indicate an improvement compared to the OL run (up to a maximum of 1), negative NIC values indicate a deterioration compared to the OL run.

2.5 Reference data

We used a range of reference data for assessing the impact of the different DA methods on different simulated variables. The vegetation and carbon cycle representation were evaluated via the gross primary productivity (GPP), whereas the hydrological component was evaluated via evapotranspiration (ET), soil moisture (SM), and runoff, either using in situ data or as spatially gridded satellite-based products.

We matched all reference data to the model grid (0.25°) by averaging (for gridded datasets) or nearest neighbour matching (for in situ data). Where available, evaluations were performed using daily model output, otherwise we averaged the model output to the temporal resolution of the reference product. In the bias-blind DA, some variables contained strong trends in the first DA year (2002), caused by the induced climatology changes. We therefore limited the evaluation to 2003–2019.

2.5.1 FluxSat GPP

FluxSat (Joiner and Yoshida, 2021) provides global daily estimates of GPP retrieved from the *Moderate Resolution Imaging Spectroradiometer* (MODIS). The retrieval is based on an empirical light use efficiency model that estimates GPP via an artificial neural network (ANN) approach. The ANN was trained using in situ estimates of GPP from eddy covariance towers (FLUXNET). FluxSat agrees well with independent eddy covariance tower measurements (Joiner and Yoshida, 2020), and has been shown to outperform other GPP retrieval approaches (Joiner et al., 2018). Since the GPP estimates of FluxSat are based on data from optical sensors (although different from the ones used in our study), they might not be fully independent of the assimilated LAI observations, and especially correlation metrics might overestimate the DA skill improvements.

https://doi.org/10.5194/egusphere-2022-1137
Preprint. Discussion started: 20 December 2022

2.5.2 SIF

Sun-induced fluorescence (SIF) is a direct measure of photosynthetic activity and is mostly linearly correlated to GPP (Frankenberg et al., 2011) and ET (Maes et al., 2020). It is commonly used to evaluate improvements in the representation of GPP due to LAI data assimilation (Leroux et al., 2018; Kumar et al., 2019b; Albergel et al., 2020). We used a fused dataset from the *SCanning Imaging Absorption SpectroMeter for Atmospheric CHartographY* (SCIAMACHY) and the *Global Ozone Monitoring Experiment-2* (GOME-2) (Wen et al., 2021), which provides monthly global SIF estimates at a 0.05° resolution. Hence, the comparison with OL and DA runs was performed on monthly averages of modelled GPP. In contrast to FluxSat GPP, SIF is independent of the assimilated LAI observations, since it uses a different retrieval approach. Since SIF is only an indicator for GPP, but not a direct estimate, we evaluated it only in terms of R and R_{anom}, but not RMSD.

2.5.3 GLEAM ET

The Global Land Evaporation Amsterdam Model v3 (GLEAM; Martens et al., 2017; Miralles et al., 2011) calculates ET as a combination of potential evaporation (based on the Priestley-Taylor equation), stress (based on a soil moisture model and the assimilation of microwave-based satellite soil moisture and vegetation optical depth), and interception (based on the Gash model). We used version 3.6b, as it provides data in our evaluation period (2003-2019) and is not relying on reanalyses as forcing data. The GLEAM ET does not rely on optical data for dynamic inputs and is thus largely independent of the assimilated CGLS LAI.

2.5.4 ESA CCI soil moisture

The *European Space Agency* (ESA) *Climate Change Initiative* (CCI) soil moisture (SM) v07.1 (Dorigo et al., 2017) dataset is a merged product combining soil moisture retrievals from a multitude of satellites. We use the COMBINED product which includes soil moisture from passive satellites retrieved with the Land Parameter Retrieval Model (LPRM; Owe et al., 2008), and soil saturation from active satellites retrieved with the TU Wien change detection method (Wagner et al., 1999; Naeimi et al., 2009).

The merging is based on a variance-weighted average, with error variances obtained from a triple collocation error characterisation (Gruber et al., 2019). Recent releases also include a homogenisation of breaks that may be introduced during the merging (Preimesberger et al., 2020). The merging process also uses soil moisture estimates from the *Global Land Data Assimilation System* (GLDAS; Rodell et al., 2004) as a scaling reference, and the climatology of the final product is therefore the climatology of GLDAS. As such, we performed comparisons to ESA CCI SM only in terms of anomaly correlations.

2.5.5 ISMN soil moisture

The International Soil Moisture Network (ISMN; Dorigo et al., 2021, 2011, 2013) provides in situ soil moisture data from over 70 soil moisture sensor networks around the globe. We calculated daily averages of in situ soil moisture data from the depths 0 cm to 10 cm (SM1) and 10 cm to 40 cm (SM2) from all networks providing station data within our modelling domain (see

https://doi.org/10.5194/egusphere-2022-1137
Preprint. Discussion started: 20 December 2022

Table A1). Only data with quality flag "good" have been used, and we discarded stations with less than 1000 days of valid data within our evaluation period. Metrics were computed based on a nearest neighbour matching between ISMN stations and model grid coordinates, and in case of multiple stations per model grid cell we averaged the metrics of these stations to obtain a single value per model grid cell. Since soil moisture climatology and absolute values strongly depend on sub-grid scale factors like slope and soil texture, we only compared the in situ values in terms of anomaly correlation R_{anom}.

2.5.6 GRDC runoff

To evaluate the effects of the assimilation on modelled runoff, we used monthly river discharge station data from the Global Runoff Data Centre (GRDC; Koblenz, Germany). The station basins were derived from the provided watershed boundaries (GRDC, 2011).

The comparison of modelled total (surface + subsurface) runoff to station river discharge followed the approach of Koster et al. (2014) and Koster et al. (2018), who compared river discharge with 10-daily basin-averaged runoff. We restricted the analysis to 271 stations in Europe with a record of more than 10 years and a basin area between 625 km^2 and 100,000 km^2. The lower bound follows Kumar et al. (2014), the upper bound was increased compared to Kumar et al. (2014) and Koster et al. (2018) in order to have more available stations in southern Europe (mainly Spain). We account for the larger area by using monthly averages instead of the 10-daily averages that were used by Koster et al. (2018). Basins with a Pearson correlation of less than 0.4 with respect to the OL run were excluded, so that the evaluation was not hampered by basins that are likely strongly affected by unmodelled processes (e.g., damming or irrigation).

2.5.7 Site data from Majadas

The ecosystem research site Majadas de Tiétar (Casals et al., 2009) is located in the center of the Iberian Peninsula at $39°56'25''$N $5°46'29''$W and categorised as a semi-arid savanna type ecosystem (El-Madany et al., 2018) with a canopy height of 8.7 ± 1.25 m, and a fractional canopy cover is $23.0 \pm 5.3\%$ (Bogdanovich et al., 2021). In the land cover map used in the model, the grid cell containing the research site is classified as "savanna". The mean annual temperature at the site is about 650 mm with a large inter-annual variability. The mean LAI at the site changes strongly throughout the year between 0.55 — 2.15 $\mathrm{m^2 m^{-2}}$ with lowest values during summer and highest values during late spring. The soil is an Abruptic Luvisol with a sandy upper layer (Nair et al., 2019). In the model, the grid cell containing the research site uses parameters for a loamy sand texture.

The research site consists of three eddy covariance towers with non-overlapping footprints climatologies and similar instrumental setups (El-Madany et al., 2021). For this analysis, the data of the tower with the FLUXNET ID ES-LM1 are used. A detailed description of the instrumental setup and data processing can be found in El-Madany et al. (2018, 2021). In short, the soil moisture data are collected with four profile probes enviroSCAN (Sentek) measuring at 10, 20, 30, 50 and 100 cm plus a ML3 (Delta T) sensor at 5 cm close to each profile probe. The soil moisture data were further aggregated to depth levels representing the Noah-MP soil moisture layers for each of the 4 profiles.

https://doi.org/10.5194/egusphere-2022-1137
Preprint. Discussion started: 20 December 2022

Eddy covariance data where collected at 20 Hz with a R3-50 (Gill) and a LI-7200 CO2 and H2O gas analyser (Licor Bioscience) at 15 m above ground. Raw data were processed with EddyPro (Fratini and Mauder, 2014) to calculate fluxes of ET and CO2 at half hourly intervals. Subsequently, u*-threshold estimation, gap-filling and flux partitioning was applied using REddyProc (Wutzler et al., 2018). The resulting continuous time-series of ET and GPP were aggregated together with other meteorological parameters to hourly timestamps, from which daily averages were computed.

2.6 Evaluation of short-term DA effects

The bias between observations and forecasts leads to biased update steps. To estimate how strongly the biased updates affect different model variables, we examined forecast differences between one day after the observation time (i.e., one day after the DA update) and one day before the observation time (i.e., one day before the DA update). For each pixel and month, we calculated the median of these *after-before* differences over the years 2003-2019 and normalised it with the monthly standard deviation of the variable values over the same multi-year time range (as a measure of the local within-month variation). The normalisation facilitates a comparison of the relative effect of the update over different months and locations. The *after-before* differences were computed for both the OL (without applying the DA update) and the DA simulation for multiple variables: when the DA *after-before* differences deviated from those of the OL, then the biased update did propagate to the variable in question. The results will be presented as spatial median values across the study domain.

The biased updates can also lead to unphysical model drift back towards the model equilibrium state directly after each DA update step. To estimate this effect, we examined forecast differences between two days after the observation time (i.e., two days after the DA update) and one day after the observation time, again using normalised monthly median differences. Since there is no DA update step in between, these *after-after* differences are pure model forecast differences and do not directly contain DA update effects. In the OL, these forecast differences are a natural response to the past initial conditions and forcings, whereas in the DA, these forecast differences are also informed by a past (possibly biased) DA update in the initial conditions. Deviations between the DA and the OL *after-after* differences indicate that the short-term model forecasts after a DA update contain physically unreasonable drift artefacts.

3 Results

3.1 Mean impact of bias-blind DA

Figure 1 compares mean values of OL and bias-blind DA results (relative to mean OL values) for different variables, for the months of April through October across 17 years (2002–2019). The bias-blind DA decreases growing-season LAI over large parts of the domain or has a neutral impact. It only increases in the Alps and the Scandinavian Mountains. The regions with a large change in mean LAI are mostly semi-arid and include the Iberian Peninsula, Northern Africa, the Middle East, Turkey, and Ukraine, where modelled LAI is much higher than observed LAI, and modelled LAI is therefore strongly decreased by the

https://doi.org/10.5194/egusphere-2022-1137
Preprint. Discussion started: 20 December 2022

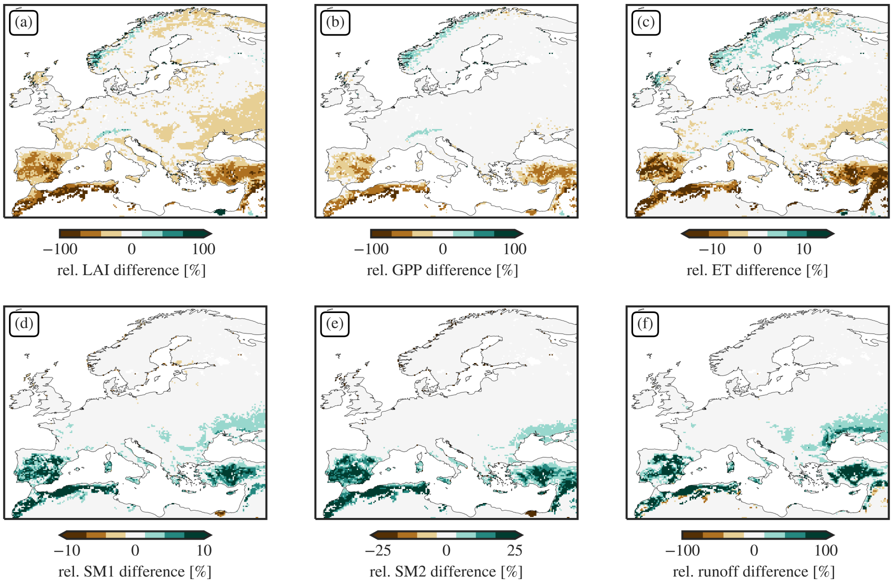

Figure 1. Relative differences between temporal mean values of OL run and bias-blind DA run for (a) LAI, (b) GPP, (c) ET, (d) SM1 (0–10 cm), (e) SM2 (10–40 cm), and (f) runoff, for the months of April through October 2002–2019. **Note the different colour bar ranges**.

bias-blind DA. In contrast, LAI increases in the Nile delta, because the lack of irrigation forcing limits the model's ability to grow vegetation.

Differences in mean GPP show similar patterns, but with a weaker impact overall, especially in Central and Eastern Europe. One exception is the Nile delta, where growing-season GPP decreases while LAI increases.

Relative differences in mean ET are much lower (note the different colour bar range), but with similar large-scale patterns as for GPP. On the Iberian Peninsula, the patterns differ slightly: the largest relative differences are in the Western part, mainly over the Duero and Tajo basins. Over Scandinavia, ET increases, except for the northernmost parts.

ET links the vegetation model to the hydrology model; consequently, the LAI assimilation also affects soil moisture and runoff. A reduction in LAI and hence transpiration leads to a reduction in soil moisture depletion. The effect is larger on deeper soil moisture layers than on surface soil moisture since the deeper layers are more strongly coupled with transpiration. In regions with large LAI biases, the relative increase in mean SM2 is about 20%. For runoff, the relative increase even reaches 100%.

3.2 Evaluation of DA impacts on GPP

The impact of bias-blind and bias-aware LAI DA on GPP is shown in figures 2 and 3, respectively. Bias-blind LAI DA strongly improves GPP estimates in terms of RMSD and R with FluxSat GPP and SIF (only R), over most of the domain, except in regions where the LAI bias is very large. In these regions, R with SIF degrades almost everywhere, and GPP RMSD and R

https://doi.org/10.5194/egusphere-2022-1137
Preprint. Discussion started: 20 December 2022

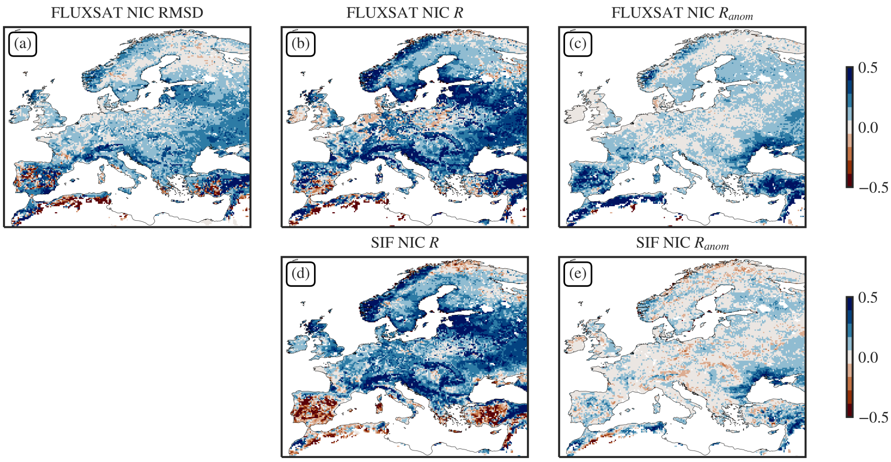

Figure 2. Maps of GPP NICs for the bias-blind DA for (a) RMSD with FluxSat, (b) R with FluxSat, (c) R_{anom} with FluxSat, (d) R with SIF, and (e) R_{anom} with SIF.

with FluxSat degrades for some grid cells. The GPP R_{anom} with FluxSat improves in most areas, especially in those with large
325 LAI biases. Similarly, the highest improvements in R_{anom} with SIF are found in areas with large LAI biases, excluding the Iberian Peninsula.

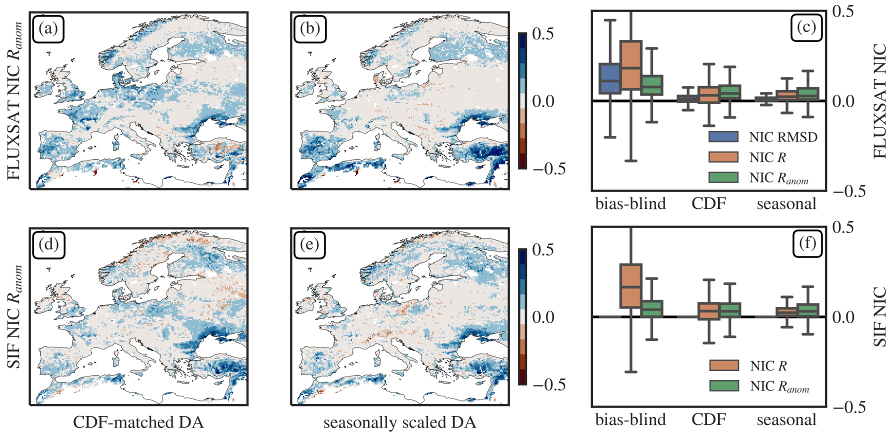

Figure 3. Top row: Maps of NIC R_{anom} with FluxSat GPP for (a) the CDF-matched DA, (b) the seasonally scaled DA, and (c) box plots of NICs for RMSD, R, and R_{anom} with FluxSat GPP for all three DA runs. Bottom row: Maps of NIC R_{anom} with SIF for (d) the CDF-matched DA, (e) the seasonally scaled DA, and (f) box plots of NICs for R and R_{anom} with SIF for all three DA runs. The upper limit of the box plots showing NIC R for the bias-blind DA (around 0.8 for FluxSat, 0.7 for SIF) has been cut here to facilitate a better comparison with the bias-aware runs.

https://doi.org/10.5194/egusphere-2022-1137
Preprint. Discussion started: 20 December 2022

In the scaled LAI DA runs, the improvements in R_{anom} are similar, but the improvements in RMSD and R are lower, as summarised in Figure 3c and f. The CDF-matched DA improves GPP R_{anom} with FluxSat over most regions, but not as strongly as the bias-blind DA (Figure 3a). The seasonally scaled DA has largest improvements in regions with large LAI bias, where it outperforms the CDF-matched DA, and has a low impact over the rest of the domain (Figure 3b). For SIF, the patterns in NIC R_{anom} are similar for all three runs (Figure 3d-e).

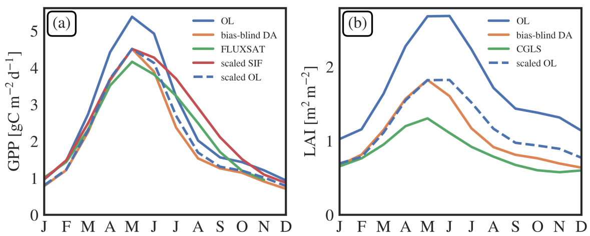

Figure 4. Mean seasonal cycles of (a) GPP and SIF, and (b) LAI, averaged over all model grid cells south of 42° where the relative LAI difference is lower than -30% (see Figure 1a). SIF and "scaled OL" have been rescaled to have the same maximum as "bias-blind DA" to ease the comparison of the shapes of the curves.

The decrease in correlation with SIF in the regions with large bias indicate that the agreement in the seasonal cycles of SIF and GPP deteriorate. We therefore examined the seasonal cycle of model GPP and reference datasets for the high-bias regions in the southern part of the domain. Figure 4 shows the mean seasonal cycles of GPP, SIF, and LAI, averaged over all model grid cells with large positive LAI bias with respect to the observations in the southern part of the modelling domain.

The OL climatology has a higher and sharper peak than the reference FluxSat or SIF data. The bias-blind DA improves the GPP magnitude in spring to be in line with FluxSat GPP, and leads to a sharper spring peak in the seasonal cycle of GPP than in the OL (orange line vs. dashed blue line in Figure 4). The low summer-fall tail of the GPP peak in the bias-blind DA climatology is considerably lower than that of the FluxSat or SIF reference datasets.

The steeper seasonal cycle of GPP for the bias-blind DA experiment is induced by a similar change in the seasonal cycle of LAI. This is partly caused by the earlier decrease of LAI in the observations than in the model, but also by the change in model drift towards the equilibrium state throughout the season. In spring, the model drifts more strongly towards the OL value, as indicated by the much more pronounced sawtooth pattern (Figure 9), and the bias-blind DA does not manage to keep the LAI close to the observations. As a consequence, the spring LAI peak in the bias-blind DA is sharper than in both the OL and the observations (Figure 4b).

3.3 Evaluation of DA impact on model hydrology

The impact of bias-blind and bias-aware LAI DA on hydrological ET and runoff fluxes is presented in Figures 5 and 6, respectively.

https://doi.org/10.5194/egusphere-2022-1137
Preprint. Discussion started: 20 December 2022

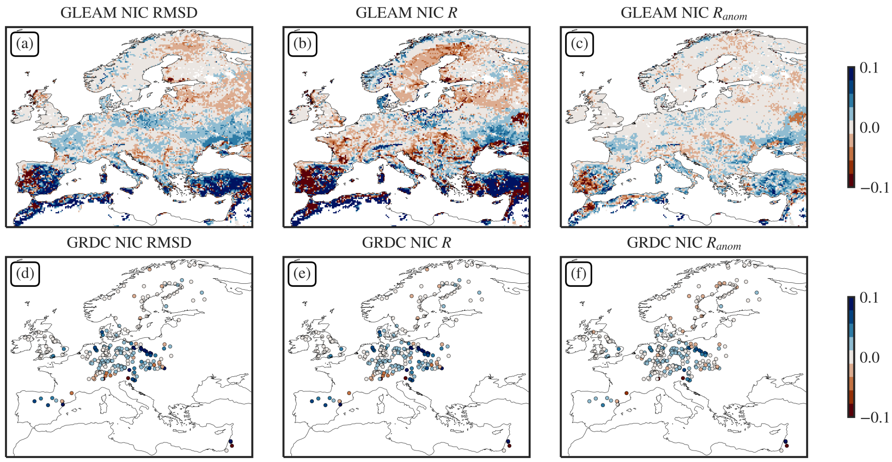

Figure 5. Top row: Maps of ET NICs for the bias-blind DA for (a) RMSD with GLEAM, (b) R with GLEAM, and (c) R_{anom}. Bottom row: Maps of runoff NICs for the bias-blind DA for (d) RMSD with GRDC, (e) R with GRDC, and (f) R_{anom} with GRDC. Note the different colour bar ranges, especially compared to Figure 2

.

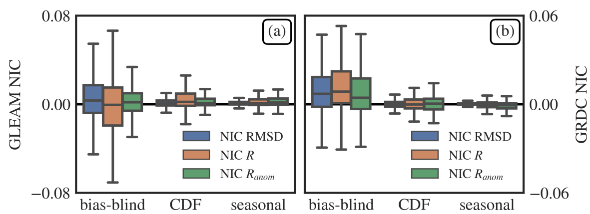

Figure 6. Box plots of RMSD, R, and R_{anom} for all three DA runs with (a) GLEAM ET and (b) GRDC runoff.

The ET shows mixed results in terms of RMSD, R, and R_{anom} with GLEAM ET (Figure 5a-c). The bias-blind DA improves RMSD, R, and R_{anom} over most of Turkey and the eastern Iberian Peninsula, but degrades over the western Iberian Peninsula and eastern Turkey. In central and eastern Europe, RMSD improves over most agricultural regions, but R mostly degrades over these regions. In northern Europe, both RMSD and R degrade compared to the OL run. The runoff estimates mainly improve in terms of RMSD, R, and R_{anom} with GRDC station data, especially in Spain and central Europe, but there is a negative impact in the Alps and Scandinavia (Figure 5c-e). The rescaling techniques decrease both positive and negative DA impact on ET and runoff, resulting in very low NICs (Figure 6a-b).

Finally, the DA results are evaluated in terms of surface (0-10 cm) and deeper (10-40 cm) soil moisture against in situ data and the ESA CCI SM in Figure 7. Because of the sparse spatial coverage, the evaluation with ISMN lacks a clear spatial pattern. The median R_{anom} is slightly positive for SM1 and SM2 for the bias-blind LAI DA, whereas the CDF-matched DA tends to

https://doi.org/10.5194/egusphere-2022-1137
Preprint. Discussion started: 20 December 2022

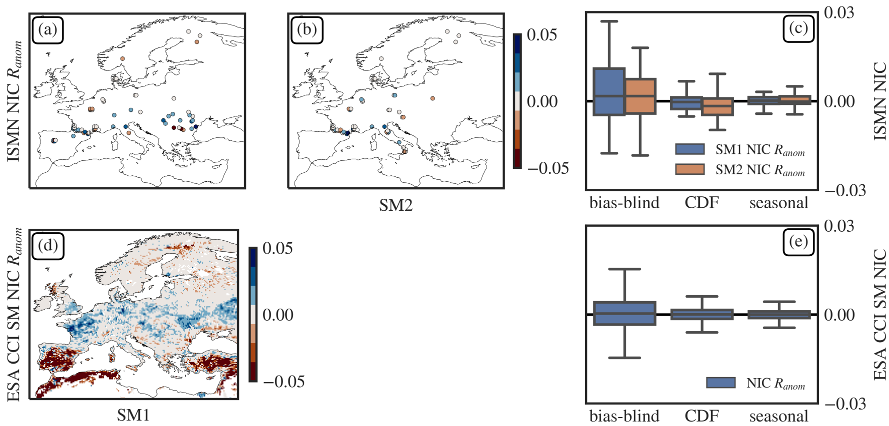

Figure 7. Top row: Maps of NIC R_{anom} with ISMN for the bias-blind DA for (a) SM1 (0-10 cm) R_{anom} and (b) SM2 (10-40 cm) R_{anom}, and (c) box plots of NIC R_{anom} with ISMN for SM1 and SM2 and all three DA runs. Bottom row: (d) Map of NIC R_{anom} with ESA CCI SM for the bias-blind DA and (e) box plots of NIC R_{anom} with ESA CCI SM for all three DA runs. Note the different color bar range compared to Figure 2 and Figure 5.

decrease R_{anom}, but with a lower impact than in the bias-blind case (Figure 7c). The seasonally scaled LAI DA has only little impact on SM1 and SM2.

The comparison with the satellite-based ESA CCI SM presents a spatially more complete picture of R_{anom} decrease in regions with large LAI bias (Figure 7d). R_{anom} also decreases over several mountain ranges and in Scandinavia, but increases over agricultural areas in central Europe. The median NIC (Figure 7e) is small for all experiments, with lower NIC spread for the rescaled DA runs.

3.4 Example I: Majadas site

To interpret the strong relative differences found in the previous section, we confront time series of multiple model variables with in situ data for the Majadas site in Figure 8. We chose the years 2015 through 2017 as example, because of (1) the availability of in situ data, and (2) considerable interannual variability in OL and observed LAI.

The OL and CGLS LAI show some similar features in their temporal patterns, but timing and magnitude disagree. Both show peaks in late spring or summer and reach their minimum in early autumn, followed by a small increase (Figure 8a). They also agree that the peak in spring/summer 2016 is the highest within these 3 years. However, the CGLS LAI reaches its maximum already start of May, and then rapidly decreases, while the OL reaches its maximum later, and decreases more slowly. Additionally, the OL has a higher overall LAI, and a lower interannual variation in maximum peak than the CGLS LAI. The magnitude of the spring maxima and the summer minima also match the observed maximum and minimum value better ($2.15\,\mathrm{m^2 m^{-2}}$ and $0.55\,\mathrm{m^2 m^{-2}}$, lower and upper thick grey line in Figure 8a, respectively). The large differences in summer lead to pronounced sawtooth patterns in the bias-blind DA results, showing that the model has a strong drift back towards the

https://doi.org/10.5194/egusphere-2022-1137
Preprint. Discussion started: 20 December 2022

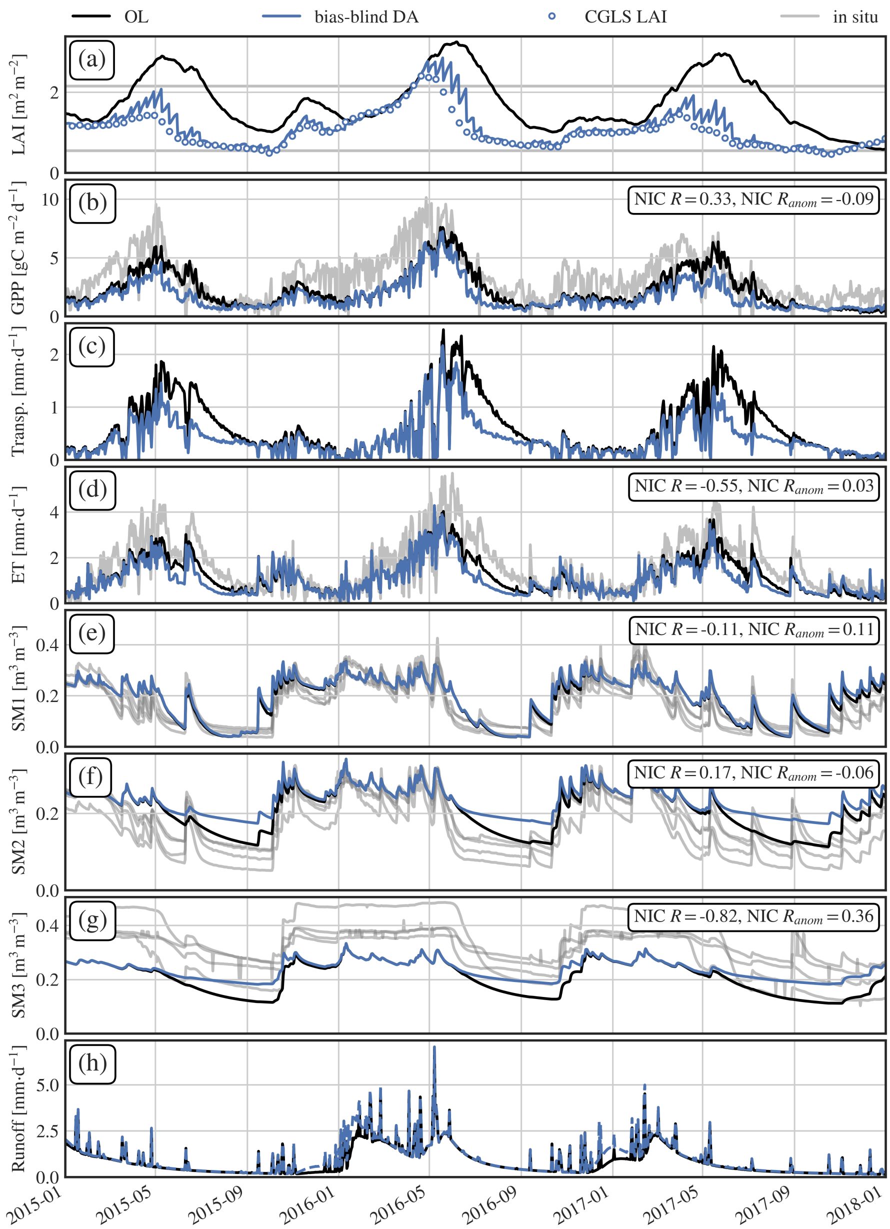

Figure 8. Time series of OL (black) and bias-blind DA (blue dashed) results for (a) LAI, (b) GPP, (c) transpiration, (d) ET, (e) SM1 (0-10 cm), (f) SM2 (10-40 cm), (g) SM3 (40-100 cm), and (h) total runoff (surface + subsurface) for the model grid cell containing the Majadas site (39.875°, -5.875°). Panel (a) also shows the assimilated LAI observations (blue dots) and the minimum and maximum observed LAI at the site (grey lines). For the other panels, in situ data from the Majadas site are also shown (grey lines), if available, and the NICs for R and R_{anom} (calculated based on the full period of data availability) are indicated in the panels.

https://doi.org/10.5194/egusphere-2022-1137
Preprint. Discussion started: 20 December 2022

equilibrium state after each DA update. The large differences in summer lead to pronounced sawtooth patterns in the bias-blind DA results, showing that the model has a strong drift back towards the equilibrium state after each DA update.

The decrease of summer LAI in the DA also induces a decrease of summer GPP (Figure 8b). This increases R with the in situ flux tower measurements, but slightly decreases R_{anom}. A better agreement can be seen in spring 2015, where observed and analysed GPP decline faster than the OL, and in spring 2017, where the OL GPP increases until mid May, while DA and observations stay at the same level as in April. The differences in overall magnitude between the in situ data and the model might be caused by representativeness errors, for example, differences in the assumed canopy cover for the savanna land cover class in the model and the canopy cover at the Majadas site.

Transpiration strongly decreases in summer as a consequence of the lower LAI (Figure 8c), which leads to a lower ET (Figure 8d). For the latter, correlation with the in situ data decreases, in agreement with the decreased correlation with GLEAM ET in the western Iberian Peninsula seen in Figure 5a, while the anomaly correlation slightly increases.

Soil moisture also increases, with a larger effect in the deeper layers (Figure 8e-g). The first layer (0-10 cm) is only slightly affected, but the deeper layers (layer 2 = 10-40 cm, layer 3 = 40-100 cm, layer 4 100-200 cm (not shown)) are much wetter in summer and autumn, caused by a slower drying rate. These large changes are hard to compare across scales, since the soil moisture climatology depends strongly on local factors like soil texture or topography (Dong and Ochsner, 2018).

The changes in the model LAI also affect surface and subsurface runoff (Figure 8h). The main difference in the example grid cell is an increased subsurface runoff for the analysis in winter 2016 and 2017.

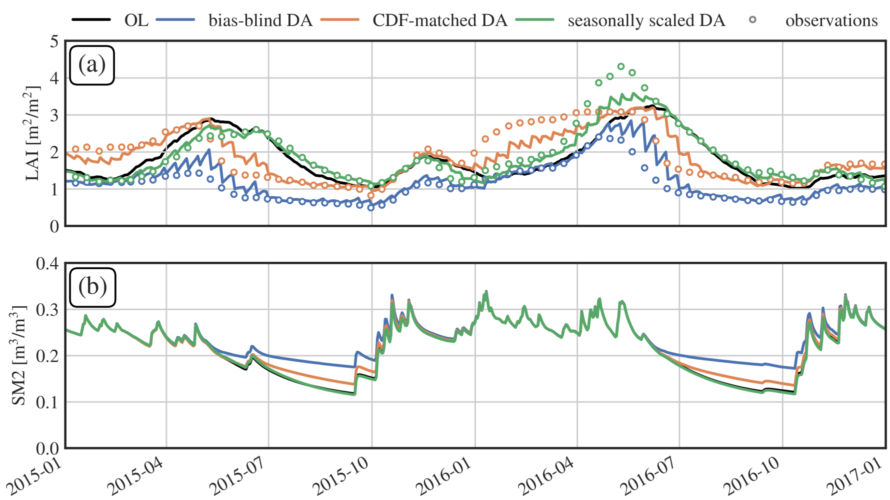

Figure 9. Time series of (a) LAI and (b) SM2 (10-40 cm) for all DA runs for the Majadas grid cell. Panel (a) includes the (potentially rescaled) observations that were assimilated in each run (coloured dots, dot colours correspond to line colours).

Figure 9 shows that the two rescaling techniques studied in this paper reduce the difference between OL and analysis LAI. In the CDF-matched DA, winter LAI is higher than the OL, while in autumn LAI drops faster than in the OL. This leads to

https://doi.org/10.5194/egusphere-2022-1137
Preprint. Discussion started: 20 December 2022

differences in layer 2 soil moisture in autumn, although they are not as strong as in the bias-blind DA. The seasonally scaled DA follows the OL more closely. The rescaled runs still contain the sawtooth pattern that was present in Figure 8a, but often with a less steep drift between updates, and with seasonally varying directions. Especially the seasonal rescaling performs well at suppressing the sawtooth pattern.

3.5 Example II: Nile delta

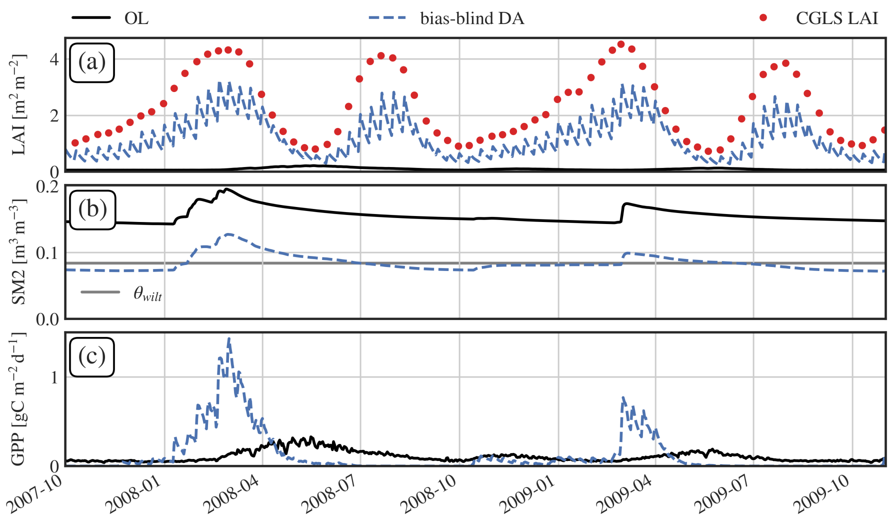

Figure 10. Time series of (a) LAI, (b) SM2 (10-40 cm), and (c) GPP for the OL and the bias-blind DA for a model grid cell in the Nile delta $(31.125°, 30.875°)$.

As another example we examined the Nile delta, where observed LAI strongly exceeds OL LAI, but summer GPP strongly decreases compared to the OL (see Figure 1). The low vegetation in the OL is caused by a lack of irrigation in the model, which results in water limitations for vegetation growth. Figure 10a shows that the bias-blind DA strongly increases LAI to follow the observations more closely However, it also strongly decreases SM2 (Figure 10b), such that the wettest conditions in the bias-blind DA are still drier than the driest conditions in the OL. As a consequence, SM2 falls below the model wilting point in summer, and the model disables photosynthesis due to water stress (Figure 10c). This decouples analysed LAI and GPP in summer, and explains the decrease in April to October GPP seen in Figure 1. Instead of correcting the root cause for the LAI underestimation, the DA worsens the problem here.

3.6 Evaluation of short-term DA effects

To assess the degree of propagation of the LAI sawtooth pattern to flux estimates, we examined differences in the magnitude of LAI, GPP and ET between one day after the DA update step (not applied for the OL run) and one day before the DA update step (*after-before*), and two days after the DA update step and one day after the DA update step, (*after-after*, Figure 11).

https://doi.org/10.5194/egusphere-2022-1137
Preprint. Discussion started: 20 December 2022

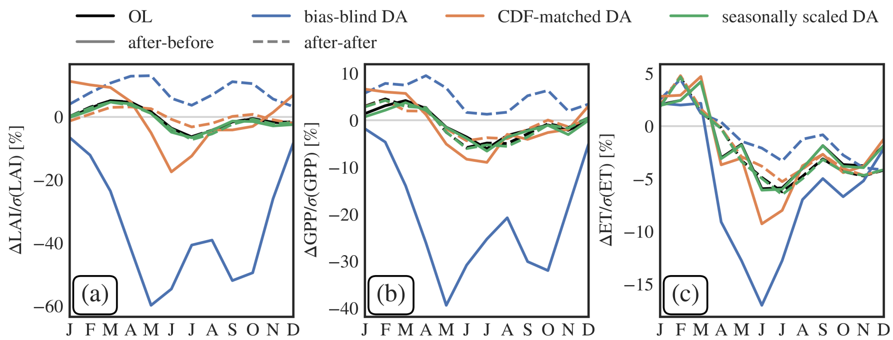

Figure 11. Normalised monthly median day-to-day forecast differences for (a) LAI, (b) GPP, and (c) ET. The differences are computed as the forecast value at 1-day after DA (not applied for OL) minus that of 1-day before DA (*after-before*, solid) and 2-day after DA minus 1-day after DA (*after-after*, dashed) for the OL (black), the bias-blind DA (blue), the CDF-matched DA (orange) and the seasonally scaled DA (green). The median was calculated from all grid cells south of 42°N at which the relative LAI difference between OL and bias blind DA (see Figure 1) is below -30%. For each grid cell and month, the median was normalised with the monthly standard deviation of the variable for this grid cell. The graph shows the median results across 17 years (2003-2019).

The seasonal cycle of the differences in the OL reflects the derivative of the seasonal cycle of the simulated variables (and is evidently very similar for *after-before* and *after-after* samples). The differences peak at the inflexion points of LAI and GPP in March and July, and cross the zero line in May and December, when LAI and GPP reach their maximum and minimum, respectively (Figure 11a-b, also compare Figure 4 for LAI and GPP seasonal cycle). For ET, the seasonal cycle of the difference is shifted compared to LAI and GPP, but has otherwise similar features (Figure 11c).

The bias-blind DA significantly impacts the *after-before* and *after-after* differences. As a consequence of the strongly biased LAI updates that always pull model LAI down, the *after-before* differences are strongly negative in summer. This is most pronounced for LAI, where the differences reach almost 60% of the monthly LAI standard deviation, but also for GPP, the differences reach up to 40% of the monthly GPP standard deviation. For ET, the differences are lower and only reach up to 15%. In contrast, the *after-after* differences are positive throughout the year for LAI and GPP. This means that even in late summer and autumn, when LAI and GPP should have a decreasing trend, LAI and GPP in the bias-blind DA have an upwards drift after each DA update. For ET, the effect is lower, but the *after-after* differences in summer are still higher than in the OL run.

The OL and the seasonally scaled DA run have similar seasonal cycles for normalised *after-before* and *after-after* differences. This indicates that with the seasonal scaling, the DA update does not introduce a bias into the flux estimates. The CDF-matched DA differences are also close to the OL, but they cross the zero line earlier and are lower throughout summer, in agreement with the earlier peak and more pronounced sawtooth pattern compared to the seasonal rescaling seen in Figure 9a.

https://doi.org/10.5194/egusphere-2022-1137
Preprint. Discussion started: 20 December 2022

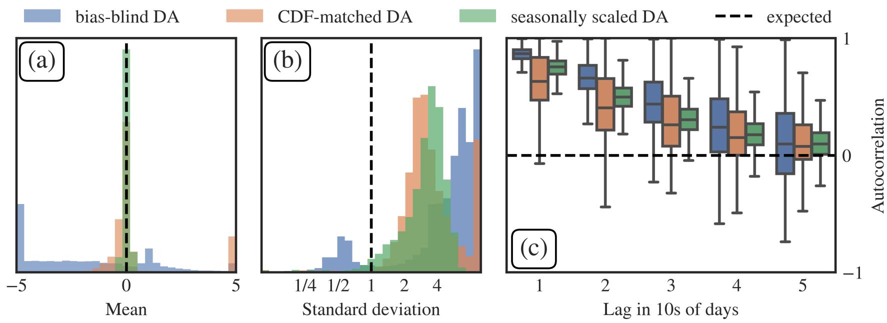

Figure 12. Spatial distributions of the temporal (a) mean, (b) standard deviation, and (c) autocorrelation of the innovations, across all model grid cells. (a-b) Values for means and standard deviations outside the plot range of the histograms have been added to the first and last bin, respectively. (c) The autocorrelation is computed for multiple lags of 10 days.

3.7 DA diagnostics

Figure 12 shows distributions of innovation statistics across the modelling domain and show that the innovation sequence is not standard normal for the bias-blind DA. As a consequence of the higher LAI in the model, the normalised innovation mean is strongly negative (Figure 12a), and the absolute values of the innovations are large (Figure 12b). The autocorrelation is also high (Figure 12c) because subsequent updates point in the same direction.

The rescaling improves the internal diagnostics of the DA system. Although there is still a sawtooth pattern (Figure 9), the assumption of zero mean innovations is met and rescaling helps to reduce the innovation variance (Figure 12b) and the autocorrelation (Figure 12c) compared to the bias-blind DA run.

4 Discussion

4.1 General impacts of bias-blind and bias-aware DA

Our analysis shows that large biases between Noah-MP modelled LAI and CGLS LAI exist. This includes bias in the length of the growing season, which might be caused by processes not included in the model (e.g. agriculture), but also strong bias in the LAI magnitude. It is most pronounced over dry areas in the southern part of the modelling domain, in line with results of Li et al. (2022), who also found an overestimation of LAI by Noah-MP's dynamic vegetation model with respect to MODIS LAI in this area. Noah-MP is not unique in this respect, studies with other LSMs have also found model deficiencies in dry regions (Dahlin et al., 2015; MacBean et al., 2015; Fox et al., 2018; Mahmud et al., 2021).

The bias-blind LAI DA therefore has a strong impact on the vegetation model state and fluxes. Where LAI bias is large, the bias-blind DA induces strong changes in GPP magnitude, which are mostly reducing RMSD with FluxSat, in agreement with results found by Kumar et al. (2019b) and Albergel et al. (2020) for similar GPP reference datasets. Anomaly correlation

https://doi.org/10.5194/egusphere-2022-1137
Preprint. Discussion started: 20 December 2022

improvement for FluxSat and SIF differs, but both show generally a positive impact. The difference might be due to the dependence of both the assimilated LAI observations and the FluxSat GPP retrievals on reflectances from optical satellite sensors, which might inflate anomaly correlations.

The strong impacts of the bias-blind DA also propagate to the model hydrology. Results for ET estimates are mixed: RMSD and R_{anom} with GLEAM generally improve, especially over Turkey, the western Iberian Peninsula, and agricultural regions, but R deteriorates over most of the domain. In contrast, runoff estimates improve compared to the GRDC discharge data. Anomaly correlation with ESA CCI SM also improves over agricultural regions, but decreases over high-bias regions and northeastern Europe. However, in northeastern Europe the Noah-MP model-only SM estimates outperform ESA CCI SM when comparing to in situ sites (Heyvaert et al., 2022, in review), probably due to the lower signal to noise ratio of soil moisture retrievals over dense vegetation and organic soils (Gruber et al., 2019).

The large changes to the root-zone soil moisture climatology are hard to assess directly, because of the scale difference between in-situ data and model grid cells. However, in strongly irrigated areas the change in soil moisture climatology leads to a decrease in soil moisture, even though the bad model performance originates from an underestimation of soil moisture due to the lack of an irrigation process in the model. Joint updates of LAI and root zone soil moisture as done in LDAS-Monde (Albergel et al., 2017) could alleviate this problem caused by “missing” water to some extent but requires a good estimation of the coupling strength of LAI and soil moisture. The strong effect on the model hydrology might also be model-specific, because the Noah-MP model hydrology is more sensitive to vegetation than other LSMs (Maertens et al., 2021).

Even though our results for RMSD improvements in GPP and ET are similar to other studies (Kumar et al., 2019b; Albergel et al., 2020), it is important to note that none of the reference products we used are free of bias. This can be due to assumptions and errors in the underlying satellite data and retrieval algorithms in the case of satellite-based data, or due to different spatial support in the case of in situ data. Hence, whether the bias-blind DA leads to estimates closer to the “truth” remains uncertain, and evaluations with different reference products might come to different conclusions. We therefore additionally investigated effects of the DA on the model and on internal DA diagnostics.

4.2 Negative effects on optimality of DA system when ignoring bias

As an effect of "misusing" a Kalman filter for correcting biases instead of random errors, DA updates are strongly biased, leading to non-optimal DA diagnostics and a pronounced sawtooth pattern. Such sawtooth patterns are common in filter DA (e.g., Mitchell et al., 2002; Dee, 2005; Fox et al., 2018), but the strong preference for one direction and the model drift between two update steps harms estimates of other variables. GPP and ET are strongly reduced at the time of the DA update, and the short term model forecasts directly after the DA update step show unphysical upward drifts.

The sawtooth pattern also poses the danger of introducing spurious trends, in case the observation frequency changes over time (Dee, 2005). For example, if the availability of LAI observations at the Majadas site increased over time, the model would be pulled more closely to the observations, i.e. lower LAI values in the later periods than in the early period, leading to an apparent decrease in LAI. Due to the strong impact of LAI changes on soil moisture, this would also lead to a spurious wetting trend in the deeper soil layers. Such artificial trends can seriously confound trends in the resulting dataset.

https://doi.org/10.5194/egusphere-2022-1137
Preprint. Discussion started: 20 December 2022

The sawtooth pattern has also been reported by other LAI DA studies using Noah-MP (Kumar et al., 2019b; Mocko et al., 2021), and might be a problem specific to the Noah-MP vegetation model. It indicates that the model has an equilibrium LAI that is largely independent of the current model state, to which it tries to return after each DA update.

4.3 Effects of bias-aware DA

Using rescaling techniques for a priori bias correction comes at the cost of foregoing improvements in ET, runoff, and GPP. However, the rescaling techniques retain improvements of GPP anomaly correlation and limit the side effects of the LAI DA on model hydrology. The CDF-matching performs better for GPP anomalies over central Europe and for ET over the high-bias regions, since it preserves more information on the shape of the observed seasonal cycle of LAI. But due to its larger impact on ET compared to the seasonal rescaling it also changes the soil moisture climatology in deeper layers, and leads to a decrease in anomaly correlation with in situ soil moisture, especially for deeper layers. The seasonal rescaling has a better performance for GPP anomalies over the high-bias regions when using FluxSat GPP as reference, but not with SIF, which may indicate an overestimation in skill as discussed above. Overall, the seasonal rescaling minimises the DA effects on the model hydrology.

Since the bias-aware DA limits the DA to address only the random error components, filter diagnostics are more in line with standard assumptions (Desroziers et al., 2005). This facilitates a further reduction of the variance and autocorrelation of the normalised innovations to obtain an optimal filter configuration by tuning the model and observation perturbations.

The limited DA impacts and more well-behaved filter performance could be especially helpful when assimilating multiple datasets, because contrasting biases could deteriorate the ability of the DA system to find a good compromise between multiple observations and model predictions (MacBean et al., 2016). This might for example arise if variables that require more complex observation operators are assimilated, and the observation operator is calibrated to the original model climatology.

4.4 Alternatives to rescaling of observations

As an alternative to rescaling, which aims to bring the observation climatology close to the model climatology, calibration or model structural changes can bring the model climatology close to the climatology of the observations.

The vegetation model in Noah-MP consists of two parts: a photosynthesis model, which calculates how much carbon is assimilated from the atmosphere in each time step, and the dynamic vegetation model, which distributes the carbon to different plant carbon pools and calculates losses due to respiration and turnover. Previous studies found that the dynamic leaf model decreases performance compared to a prescribed LAI (Ma et al., 2017; Erlingis et al., 2021; Huang et al., 2022). Structural changes in the equations governing the leaf carbon assimilation might therefore improve the agreement of modelled and observed LAI.

A promising candidate for structural changes is the leaf carbon allocation function, which governs which fraction of the photosynthesis carbon is allocated to the leaves. In Noah-MP v4.0.1, this function decreases from 1 at LAI=0 to 0 at approximately LAI=6 with a sigmoidal-like shape. Alternative formulations have been tested by Gim et al. (2017) and Niu et al. (2020). They used sigmoidal functions with a sharp decline around a threshold LAI. This sharp decline would likely worsen the issue of the sawtooth pattern, since it increases model drift towards the equilibrium, i.e., the threshold LAI. But when treating this threshold

https://doi.org/10.5194/egusphere-2022-1137
Preprint. Discussion started: 20 December 2022

as a model parameter, these formulations open up new possibilities for calibration and parameter data assimilation, since the threshold LAI gives a more direct access to adapting the maximum LAI reached in summer. Multi-pass schemes that update the threshold based on observations, similar to Xu et al. (2021), might be able to improve the persistence of observations and alleviate the sawtooth pattern issue.

Another shortcoming of Noah-MP is its oversimplified phenology scheme, which is solely based on a land cover-specific canopy temperature threshold, ignoring other drivers of phenology like day length or water availability (e.g., Dahlin et al., 2015, 2017), or cumulative temperature effects often expressed via growing degree days (e.g., in CLM, Lawrence et al., 2011). Especially in the southern part of our modelling domain, where water partly limits vegetation growth (Hashimoto et al., 2019), more complex phenology schemes might improve the realism of the vegetation simulations. In the current scheme, the temperature threshold is almost always exceeded, leading to unrealistically long growing seasons. However, additional degrees of freedom introduced by a more complex phenology scheme can also deteriorate model predictions (Lawrence et al., 2011).

An alternative to model structural changes is calibration, which has been successful at improving vegetation models in previous studies (MacBean et al., 2015, 2016; Scholze et al., 2019; Forkel et al., 2019; Kolassa et al., 2020; Mahmud et al., 2021). In the version of the Noah-MP model that we used, the specific leaf biomass, and parameters related to leaf respiration and turnover can be tuned to modify the maximum summer LAI and thereby improve the agreement with the observations. Another option is adapting the temperature threshold used in the phenology scheme for each model grid cell separately. A spatially variable temperature threshold could serve as a proxy for day length in the phenology scheme.

Our study demonstrates that a parameter calibration that changes model LAI can strongly affect the model hydrology, as the impacts will be similar to the impacts of the bias-blind DA. These impacts might improve flux estimates, but it is unclear whether the large changes in the soil moisture climatology in deeper soil moisture layers are desirable. Parameters related to transpiration, (e.g., minimum stomatal resistance as recommended by Boussetta et al., 2013) could be adapted to limit the impact on the model hydrology. Using additional data, for example, soil moisture retrievals, can be helpful in constraining the model hydrology in this case.

The calibration can either be done as a separate step before the state update DA or can be incorporated into a joint parameter and state update DA scheme. An EnKF (as used in this study) can in principle be used for the joint updates by augmenting the control vector to contain both state variables and parameters (Evensen, 2009). If the model predictions' dependency on the parameters is highly nonlinear, particle methods might be more suitable (Frei and Künsch, 2013; van Leeuwen et al., 2019). Hybrid methods that combine the EnKF with particle methods could be used to obtain a DA system that performs well both for state updates and parameter updates (Frei and Künsch, 2013; van Leeuwen et al., 2019; De Lannoy et al., 2022).

5 Conclusions

So far, satellite LAI DA studies have mostly ignored biases between observed and modelled LAI. In this study, we evaluated how the presence of bias in a LAI DA system can impact the model hydrology and carbon uptake. Specifically, we assimilated

CGLS LAI into Noah-MP with an EnKF and we evaluated a bias-blind DA and two rescaling techniques, i.e. climatological CDF-matching and seasonal rescaling of the first two moments, to account for the biases in the DA system.

To summarise, we recommend using rescaling techniques for LAI DA in the presence of strong biases

- if the focus is not only on vegetation or the carbon cycle, but also on hydrological processes, because large LAI changes can cause unphysical impacts on model hydrology;
- if multiple datasets with contrasting biases are assimilated, since the bias-blind DA can strongly change the model climatology;
- if the DA aims at preparing the best analysis state for subsequent short-term predictions, because the abrupt update steps induce spurious short-term trends;
- if datasets with changes in observation frequency are used, because this can induce spurious long-term trends;
- if an optimal DA system in terms of Desrozier's metrics (Desroziers et al., 2005) is desired, because bias-blind DA violates basic assumptions of the Kalman filter.

The CDF-matching technique preserves more information from the signal and leads to larger improvements in GPP and ET, but worse estimates of deeper layer soil moisture. The seasonal rescaling performs best in terms of internal DA diagnostics and in limiting DA updates to improving the vegetation anomalies. The bias-aware LAI DA is suitable to provide physically consistent short-term flux estimates for numerical weather prediction models or soil moisture monitoring, or a baseline to merge historical earth observation records from multiple sensors to a long-term dataset without introducing artificial trends.

An alternative to bias-aware DA is an a priori model calibration or a joint parameter and state update DA, which would lead to model estimates of vegetation in the observation climatology, which is desirable for research on the carbon cycle. Further research is needed to correctly simulate and optimise the coupling mechanisms between the water and carbon cycle to gain the most benefit from subsequent data assimilation.

Appendix A: Used ISMN networks

Author contributions. Samuel Scherrer performed the data assimilation runs and the analysis of the results, and drafted the manuscript. Zdenko Heyvaert, Gabriëlle De Lannoy, and Michel Bechtold assisted with the setup of the LSM and the data assimilation system. Zdenko Heyvaert, Gabriëlle De Lannoy, and Michel Bechtold, Wouter Dorigo and Clement Albergel provided scientific input to the design of the study. Tarek S. El-Madany provided in situ data. All authors contributed to the final draft of the paper by providing input for the final manuscript and discussion of the results.

Competing interests. The authors declare that they have no conflict of interest.

https://doi.org/10.5194/egusphere-2022-1137
Preprint. Discussion started: 20 December 2022

Table A1. ISMN networks used for evaluation.

Network name	Country	Stations	Coverage	References/Acknowledgements
CALABRIA	Italy	5	2001-2012	Brocca et al. (2011b)
CAMPANIA	Italy	2	2000-2012	Brocca et al. (2011b)
COSMOS	Switzerland	1	2008-2020	Zreda et al. (2008, 2012)
FMI	Finland	27	2007-2022	Ikonen et al. (2016, 2018)
FR_ Aqui	France	5	2012 - 2022	Al-Yaari et al. (2018); Wigneron et al. (2018)
GTK	Finland	7	2001 - 2012	Raimo Sutinen
HOAL	Austria	33	2013-2021	Blöschl et al. (2016); Vreugdenhil et al. (2013)
HOBE	Denmark	32	2009-2019	Jensen and Refsgaard (2018); Bircher et al. (2012)
HYDROL-NET_PERUGIA	Italy	2	2010 - 2016	Morbidelli et al. (2017)
IMA_CAN1	Italy	12	2011-2015	Biddoccu et al. (2016); Raffelli et al. (2017)
IPE	Spain	2	2008-2020	Alday et al. (2020)
MOL-RAO	Germany	2	2003-2020	Beyrich and Adam (2007)
NVE	Norway	3	2012 - 2019	Norwegian water resources and energy directorate (NVE), Fred Wenger
ORACLE	France	6	1985 - 2013	Institut national de recherce en sciences et technologies pour l'environment et l'agriculture France
REMEDHUS	Spain	24	2005-2022	González-Zamora et al. (2019)
RSMN	Romania	20	2014 - 2022	Romanian National Meteorological Administration, Andrei Dimandi, Adelina Mihai
SMOSMANIA	France	22	2007 - 2021	Calvet et al. (2016); Albergel et al. (2008); Calvet et al. (2007)
STEMS	Italy	4	2015 - 2022	Capello et al. (2019); Darouich et al. (2022)
SWEX_POLAND	Poland	6	2000 - 2013	Marczewski et al. (2010)
TERENO	Germany	5	2009-2021	Zacharias et al. (2011); Bogena et al. (2018, 2012); Bogena (2016)
UDC_SMOS	Germany	11	2007 - 2011	Schlenz et al. (2012); Loew et al. (2009)
UMBRIA	Italy	13	2002 - 2017	Brocca et al. (2011a, 2008, 2009)
UMSUOL	Italy	1	2009 - 2017	Agenzia Regionale Prevenzione Ambiente - Servizio Idro-Meteo-Clima (ARPA - SIMC) and Andrea Pasquali
WEGENERNET	Austria	12	2007 - 2022	Fuchsberger et al. (2021); Kirchengast et al. (2014)
WSMN	UK	8	2011 - 2016	Petropoulos and McCalmont (2017)

https://doi.org/10.5194/egusphere-2022-1137
Preprint. Discussion started: 20 December 2022

Disclaimer.

Acknowledgements. This work was funded by FWF (Austrian Science Fund) and FWO (Research Foundation Flanders) as part of the CONSOLIDATION project (G0A7320N). We also acknowledge support from the European Space Agency Climate Change Initiative (Contract No. 4000126684/19/I-655 CCI+ Phase 2) and Land Carbon Constellation (Contract No. 4000131497/20/NL/CT) projects. Computing resources were provided by the Flemish Super Computer Center (VSC).

https://doi.org/10.5194/egusphere-2022-1137
Preprint. Discussion started: 20 December 2022

References

Al-Yaari, A., Dayau, S., Chipeaux, C., Aluome, C., Kruszewski, A., Loustau, D., and Wigneron, J.-P.: The AQUI soil moisture network for satellite microwave remote sensing validation in South-Western France, Remote Sensing, 10, 1839, 2018.

Albergel, C., Rüdiger, C., Pellarin, T., Calvet, J.-C., Fritz, N., Froissard, F., Suquia, D., Petitpa, A., Piguet, B., and Martin, E.: From near-surface to root-zone soil moisture using an exponential filter: An assessment of the method based on in-situ observations and model simulations, Hydrology and Earth System Sciences, 12, https://doi.org/10.5194/hess-12-1323-2008, 2008.

Albergel, C., Munier, S., Leroux, D. J., Dewaele, H., Fairbairn, D., Barbu, A. L., Gelati, E., Dorigo, W., Faroux, S., Meurey, C., Le Moigne, P., Decharme, B., Mahfouf, J.-F., and Calvet, J.-C.: Sequential assimilation of satellite-derived vegetation and soil moisture products using SURFEX_v8.0: LDAS-Monde assessment over the Euro-Mediterranean area, Geoscientific Model Development, 10, 3889–3912, https://doi.org/10.5194/gmd-10-3889-2017, 2017.

Albergel, C., Zheng, Y., Bonan, B., Dutra, E., Rodríguez-Fernández, N., Munier, S., Draper, C., de Rosnay, P., Muñoz Sabater, J., Balsamo, G., Fairbairn, D., Meurey, C., and Calvet, J.-C.: Data assimilation for continuous global assessment of severe conditions over terrestrial surfaces, Hydrology and Earth System Sciences, 24, 4291–4316, https://doi.org/10.5194/hess-24-4291-2020, 2020.

Alday, J. G., Camarero, J. J., Revilla, J., and Resco de Dios, V.: Similar diurnal, seasonal and annual rhythms in radial root expansion across two coexisting Mediterranean oak species, Tree Physiology, 40, 956–968, 2020.

Balsamo, G., Beljaars, A., Scipal, K., Viterbo, P., van den Hurk, B., Hirschi, M., and Betts, A. K.: A Revised Hydrology for the ECMWF Model: Verification from Field Site to Terrestrial Water Storage and Impact in the Integrated Forecast System, Journal of Hydrometeorology, 10, 623 – 643, https://doi.org/10.1175/2008JHM1068.1, 2009.

Barbu, A. L., Calvet, J.-C., Mahfouf, J.-F., and Lafont, S.: Integrating ASCAT surface soil moisture and GEOV1 leaf area index into the SURFEX modelling platform: a land data assimilation application over France, Hydrology and Earth System Sciences, 18, 173–192, https://doi.org/10.5194/hess-18-173-2014, 2014.

Bechtold, M., De Lannoy, G., Reichle, R., Roose, D., Balliston, N., Burdun, I., Devito, K., Kurbatova, J., Strack, M., and Zarov, E.: Improved groundwater table and L-band brightness temperature estimates for Northern Hemisphere peatlands using new model physics and SMOS observations in a global data assimilation framework, Remote Sensing of Environment, 246, 111 805, https://doi.org/https://doi.org/10.1016/j.rse.2020.111805, 2020.

Betts, A. K., Ball, J. H., Beljaars, A. C. M., Miller, M. J., and Viterbo, P. A.: The land surface-atmosphere interaction: A review based on observational and global modeling perspectives, Journal of Geophysical Research: Atmospheres, 101, 7209–7225, https://doi.org/https://doi.org/10.1029/95JD02135, 1996.

Beyrich, F. and Adam, W.: Site and Data Report for the Lindenberg Reference Site in CEOP - Phase 1, Berichte des Deutschen Wetterdienstes, 230, Offenbach am Main, 2007, 2007.

Biddoccu, M., Ferraris, S., Opsi, F., and Cavallo, E.: Long-term monitoring of soil management effects on runoff and soil erosion in sloping vineyards in Alto Monferrato (North–West Italy), Soil and Tillage Research, 155, 176–189, 2016.

Bircher, S., Skou, N., Jensen, K., Walker, J. P., and Rasmussen, L.: A soil moisture and temperature network for SMOS validation in Western Denmark, Hydrology and Earth System Sciences, 16, 1445–1463, 2012.

Blöschl, G., Blaschke, A., Broer, M., Bucher, C., Carr, G., Chen, X., Eder, A., Exner-Kittridge, M., Farnleitner, A., Flores-Orozco, A., et al.: The hydrological open air laboratory (HOAL) in Petzenkirchen: A hypothesis-driven observatory, Hydrology and Earth System Sciences, 20, 227–255, 2016.

Bogdanovich, E., Perez-Priego, O., El-Madany, T. S., Guderle, M., Pacheco-Labrador, J., Levick, S. R., Moreno, G., Carrara, A., Pilar Martín, M., and Migliavacca, M.: Using terrestrial laser scanning for characterizing tree structural parameters and their changes under different management in a Mediterranean open woodland, Forest Ecology and Management, 486, 118 945, https://doi.org/https://doi.org/10.1016/j.foreco.2021.118945, 2021.

Bogena, H., Kunkel, R., Pütz, T., Vereecken, H., Kruger, E., Zacharias, S., Dietrich, P., Wollschläger, U., Kunstmann, H., Papen, H., Schmid, H., Munch, J., Priesack, E., Schwank, M., Bens, O., Brauer, A., Borg, E., and Hajnsek, I.: TERENO - Long-term monitoring network for terrestrial environmental research, Hydrologie und Wasserbewirtschaftung, 56, 138–143, 2012.

Bogena, H., Montzka, C., Huisman, J., Graf, A., Schmidt, M., Stockinger, M., von Hebel, C., Hendricks-Franssen, H., van der Kruk, J., Tappe, W., Lücke, A., Baatz, R., Bol, R., Groh, J., Pütz, T., Jakobi, J., Kunkel, R., Sorg, J., and Vereecken, H.: The TERENO-Rur Hydrological Observatory: A Multiscale Multi-Compartment Research Platform for the Advancement of Hydrological Science, Vadose Zone Journal, 17, 180 055, https://doi.org/10.2136/vzj2018.03.0055, 2018.

Bogena, H. R.: TERENO: German network of terrestrial environmental observatories, Journal of large-scale research facilities JLSRF, 2, A52, https://doi.org/http://dx.doi.org/10.17815/jlsrf-2-98, 2016.

Bonan, G.: Terrestrial Biosphere Models, p. 1–24, Cambridge University Press, https://doi.org/10.1017/9781107339217.002, 2019.

Boussetta, S., Balsamo, G., Beljaars, A., Kral, T., and Jarlan, L.: Impact of a satellite-derived leaf area index monthly climatology in a global numerical weather prediction model, International Journal of Remote Sensing, 34, 3520–3542, https://doi.org/10.1080/01431161.2012.716543, 2013.

Brocca, L., Melone, F., and Moramarco, T.: On the estimation of antecedent wetness condition in rainfall-runoff modeling, Hydrological Processes, 22, 629–642, https://doi.org/10.1002/hyp.6629, 2008.

Brocca, L., Melone, F., Moramarco, T., and Morbidelli, R.: Antecedent wetness conditions based on ERS scatterometer data, Journal of Hydrology, 364, 73–87, 2009.

Brocca, L., Hasenauer, S., Lacava, T., Melone, F., Moramarco, T., Wagner, W., A, D., Matgen, P., Martínez-Fernández, J., Llorens, P., Latron, J., Martin, C., and Bittelli, M.: Soil moisture estimation through ASCAT and AMSR-E sensors: An intercomparison and validation study across Europe, Remote Sensing of Environment, 115, 3390–3408, https://doi.org/10.1016/j.rse.2011.08.003, 2011a.

Brocca, L., Hasenauer, S., Lacava, T., Melone, F., Moramarco, T., Wagner, W., Dorigo, W., Matgen, P., Martínez-Fernández, J., Llorens, P., et al.: Soil moisture estimation through ASCAT and AMSR-E sensors: An intercomparison and validation study across Europe, Remote Sensing of Environment, 115, 3390–3408, 2011b.

Calvet, J.-C., Fritz, N., Froissard, F., Suquia, D., Petitpa, A., and Piguet, B.: In situ soil moisture observations for the CAL/VAL of SMOS: the SMOSMANIA network, in: 2007 IEEE International Geoscience and Remote Sensing Symposium, pp. 1196–1199, https://doi.org/10.1109/IGARSS.2007.4423019, 2007.

Calvet, J.-C., Fritz, N., Berne, C., Piguet, B., Maurel, W., and Meurey, C.: Deriving pedotransfer functions for soil quartz fraction in southern France from reverse modeling, SOIL, 2, 615–629, https://doi.org/10.5194/soil-2-615-2016, 2016.

Capello, G., Biddoccu, M., Ferraris, S., and Cavallo, E.: Effects of tractor passes on hydrological and soil erosion processes in tilled and grassed vineyards, Water, 11, 2118, 2019.

Casals, P., Gimeno, C., Carrara, A., Lopez-Sangil, L., and Sanz, M.: Soil CO2 efflux and extractable organic carbon fractions under simulated precipitation events in a Mediterranean Dehesa, Soil Biology and Biochemistry, 41, 1915–1922, https://doi.org/https://doi.org/10.1016/j.soilbio.2009.06.015, 2009.

Crameri, F., Shephard, G. E., and Heron, P. J.: The misuse of colour in science communication, Nature communications, 11, 1–10, 2020.

https://doi.org/10.5194/egusphere-2022-1137
Preprint. Discussion started: 20 December 2022

Crow, W. T., Gomez, C. A., Sabater, J. M., Holmes, T., Hain, C. R., Lei, F., Dong, J., Alfieri, J. G., and Anderson, M. C.: Soil Moisture–Evapotranspiration Overcoupling and L-Band Brightness Temperature Assimilation: Sources and Forecast Implications, Journal of Hydrometeorology, 21, 2359 – 2374, https://doi.org/10.1175/JHM-D-20-0088.1, 2020.

Dahlin, K. M., Fisher, R. A., and Lawrence, P. J.: Environmental drivers of drought deciduous phenology in the Community Land Model, Biogeosciences, 12, 5061–5074, https://doi.org/10.5194/bg-12-5061-2015, 2015.

Dahlin, K. M., Ponte, D. D., Setlock, E., and Nagelkirk, R.: Global patterns of drought deciduous phenology in semi-arid and savanna-type ecosystems, Ecography, 40, 314–323, https://doi.org/https://doi.org/10.1111/ecog.02443, 2017.

Darouich, H., Ramos, T. B., Pereira, L. S., Rabino, D., Bagagiolo, G., Capello, G., Simionesei, L., Cavallo, E., and Biddoccu, M.: Water Use and Soil Water Balance of Mediterranean Vineyards under Rainfed and Drip Irrigation Management: Evapotranspiration Partition and Soil Management Modelling for Resource Conservation, Water, 14, 554, 2022.

De Lannoy, G. J., Bechtold, M., Albergel, C., Brocca, L., Calvet, J.-C., Carrassi, A., Crow, W. T., De Rosnay, P., Durand, M., Forman, B., Geppert, G., Girotto, M., Hendricks-Franssen, H.-J., Jonas, T., Kumar, S. V., Lievens, H., Lu, Y., Massari, C., Pauwels, V., Reichle, R., and Steele-Dunne, S.: Perspective on Satellite-Based Land Data Assimilation to Estimate Water Cycle Components in an Era of Advanced Data Availability and Model Sophistication, Frontiers in Water, p. 156, 2022.

De Lannoy, G. J. M. and Reichle, R. H.: Global Assimilation of Multiangle and Multipolarization SMOS Brightness Temperature Observations into the GEOS-5 Catchment Land Surface Model for Soil Moisture Estimation, Journal of Hydrometeorology, 17, 669–691, https://doi.org/10.1175/JHM-D-15-0037.1, 2016.

De Lannoy, G. J. M., Houser, P. R., Pauwels, V. R. N., and Verhoest, N. E. C.: State and bias estimation for soil moisture profiles by an ensemble Kalman filter: Effect of assimilation depth and frequency, Water Resources Research, 43, https://doi.org/https://doi.org/10.1029/2006WR005100, 2007a.

De Lannoy, G. J. M., Reichle, R. H., Houser, P. R., Pauwels, V. R. N., and Verhoest, N. E. C.: Correcting for forecast bias in soil moisture assimilation with the ensemble Kalman filter, Water Resources Research, 43, https://doi.org/https://doi.org/10.1029/2006WR005449, 2007b.

Dee, D. P.: Bias and data assimilation, Quarterly Journal of the Royal Meteorological Society, 131, 3323–3343, https://doi.org/https://doi.org/10.1256/qj.05.137, 2005.

Derber, J. C. and Wu, W.-S.: The Use of TOVS Cloud-Cleared Radiances in the NCEP SSI Analysis System, Monthly Weather Review, 126, 2287 – 2299, https://doi.org/10.1175/1520-0493(1998)126<2287:TUOTCC>2.0.CO;2, 1998.

Desroziers, G., Berre, L., Chapnik, B., and Poli, P.: Diagnosis of observation, background and analysis-error statistics in observation space, Quarterly Journal of the Royal Meteorological Society, 131, 3385–3396, https://doi.org/https://doi.org/10.1256/qj.05.108, 2005.

Dickinson, R. E., Shaikh, M., Bryant, R., and Graumlich, L.: Interactive Canopies for a Climate Model, Journal of Climate, 11, 2823 – 2836, https://doi.org/10.1175/1520-0442(1998)011<2823:ICFACM>2.0.CO;2, 1998.

Dong, J. and Ochsner, T. E.: Soil Texture Often Exerts a Stronger Influence Than Precipitation on Mesoscale Soil Moisture Patterns, Water Resources Research, 54, 2199–2211, https://doi.org/https://doi.org/10.1002/2017WR021692, 2018.

Dorigo, W., Xaver, A., Vreugdenhil, M., Gruber, A., Hegyiová, A., Sanchis-Dufau, A., Zamojski, D., Cordes, C., Wagner, W., and Drusch, M.: Global Automated Quality Control of In Situ Soil Moisture Data from the International Soil Moisture Network, Vadose Zone Journal, 12, vzj2012.0097, https://doi.org/https://doi.org/10.2136/vzj2012.0097, 2013.

Dorigo, W., Wagner, W., Albergel, C., Albrecht, F., Balsamo, G., Brocca, L., Chung, D., Ertl, M., Forkel, M., Gruber, A., Haas, E., Hamer, P. D., Hirschi, M., Ikonen, J., de Jeu, R., Kidd, R., Lahoz, W., Liu, Y. Y., Miralles, D., Mistelbauer, T., Nicolai-Shaw, N., Parinussa, R., Pratola, C., Reimer, C., van der Schalie, R., Seneviratne, S. I., Smolander, T., and Lecomte, P.: ESA CCI Soil Moisture for improved Earth system understanding: State-of-the art and future directions, Remote Sensing of Environment, 203, 185–215, https://doi.org/https://doi.org/10.1016/j.rse.2017.07.001, earth Observation of Essential Climate Variables, 2017.

Dorigo, W., Himmelbauer, I., Aberer, D., Schremmer, L., Petrakovic, I., Zappa, L., Preimesberger, W., Xaver, A., Annor, F., Ardö, J., Baldocchi, D., Bitelli, M., Blöschl, G., Bogena, H., Brocca, L., Calvet, J.-C., Camarero, J. J., Capello, G., Choi, M., Cosh, M. C., van de Giesen, N., Hajdu, I., Ikonen, J., Jensen, K. H., Kanniah, K. D., de Kat, I., Kirchengast, G., Kumar Rai, P., Kyrouac, J., Larson, K., Liu, S., Loew, A., Moghaddam, M., Martínez Fernández, J., Mattar Bader, C., Morbidelli, R., Musial, J. P., Osenga, E., Palecki, M. A., Pellarin, T., Petropoulos, G. P., Pfeil, I., Powers, J., Robock, A., Rüdiger, C., Rummel, U., Strobel, M., Su, Z., Sullivan, R., Tagesson, T., Varlagin, A., Vreugdenhil, M., Walker, J., Wen, J., Wenger, F., Wigneron, J. P., Woods, M., Yang, K., Zeng, Y., Zhang, X., Zreda, M., Dietrich, S., Gruber, A., van Oevelen, P., Wagner, W., Scipal, K., Drusch, M., and Sabia, R.: The International Soil Moisture Network: serving Earth system science for over a decade, Hydrology and Earth System Sciences, 25, 5749–5804, https://doi.org/10.5194/hess-25-5749-2021, 2021.

Dorigo, W. A., Wagner, W., Hohensinn, R., Hahn, S., Paulik, C., Xaver, A., Gruber, A., Drusch, M., Mecklenburg, S., van Oevelen, P., Robock, A., and Jackson, T.: The International Soil Moisture Network: a data hosting facility for global in situ soil moisture measurements, Hydrology and Earth System Sciences, 15, 1675–1698, https://doi.org/10.5194/hess-15-1675-2011, 2011.

Draper, C. S., Reichle, R. H., De Lannoy, G. J. M., and Liu, Q.: Assimilation of passive and active microwave soil moisture retrievals, Geophysical Research Letters, 39, https://doi.org/https://doi.org/10.1029/2011GL050655, 2012.

Drusch, M., Wood, E. F., and Gao, H.: Observation operators for the direct assimilation of TRMM microwave imager retrieved soil moisture, Geophysical Research Letters, 32, https://doi.org/https://doi.org/10.1029/2005GL023623, 2005.

El-Madany, T. S., Reichstein, M., Perez-Priego, O., Carrara, A., Moreno, G., Pilar Martín, M., Pacheco-Labrador, J., Wohlfahrt, G., Nieto, H., Weber, U., Kolle, O., Luo, Y.-P., Carvalhais, N., and Migliavacca, M.: Drivers of spatio-temporal variability of carbon dioxide and energy fluxes in a Mediterranean savanna ecosystem, Agricultural and Forest Meteorology, 262, 258–278, https://doi.org/https://doi.org/10.1016/j.agrformet.2018.07.010, 2018.

El-Madany, T. S., Reichstein, M., Carrara, A., Martín, M. P., Moreno, G., Gonzalez-Cascon, R., Peñuelas, J., Ellsworth, D. S., Burchard-Levine, V., Hammer, T. W., Knauer, J., Kolle, O., Luo, Y., Pacheco-Labrador, J., Nelson, J. A., Perez-Priego, O., Rolo, V., Wutzler, T., and Migliavacca, M.: How Nitrogen and Phosphorus Availability Change Water Use Efficiency in a Mediterranean Savanna Ecosystem, Journal of Geophysical Research: Biogeosciences, 126, e2020JG006 005, https://doi.org/https://doi.org/10.1029/2020JG006005, e2020JG006005 2020JG006005, 2021.

Erlingis, J. M., Rodell, M., Peters-Lidard, C. D., Li, B., Kumar, S. V., Famiglietti, J. S., Granger, S. L., Hurley, J. V., Liu, P.-W., and Mocko, D. M.: A High-Resolution Land Data Assimilation System Optimized for the Western United States, JAWRA Journal of the American Water Resources Association, 57, 692–710, https://doi.org/https://doi.org/10.1111/1752-1688.12910, 2021.

Evensen, G.: The ensemble Kalman filter: Theoretical formulation and practical implementation, Ocean dynamics, 53, 343–367, 2003.

Evensen, G.: The ensemble Kalman filter for combined state and parameter estimation, IEEE Control Systems Magazine, 29, 83–104, https://doi.org/10.1109/MCS.2009.932223, 2009.

Fairbairn, D., Barbu, A. L., Napoly, A., Albergel, C., Mahfouf, J.-F., and Calvet, J.-C.: The effect of satellite-derived surface soil moisture and leaf area index land data assimilation on streamflow simulations over France, Hydrology and Earth System Sciences, 21, 2015–2033, https://doi.org/10.5194/hess-21-2015-2017, 2017.

Fang, H., Baret, F., Plummer, S., and Schaepman-Strub, G.: An Overview of Global Leaf Area Index (LAI): Methods, Products, Validation, and Applications, Reviews of Geophysics, 57, 739–799, https://doi.org/https://doi.org/10.1029/2018RG000608, 2019.

Forkel, M., Drüke, M., Thurner, M., Dorigo, W., Schaphoff, S., Thonicke, K., von Bloh, W., and Carvalhais, N.: Constraining modelled global vegetation dynamics and carbon turnover using multiple satellite observations, Scientific Reports, 9, 1–12, https://doi.org/10.1038/s41598-019-55187-7, 2019.

Fox, A. M., Hoar, T. J., Anderson, J. L., Arellano, A. F., Smith, W. K., Litvak, M. E., MacBean, N., Schimel, D. S., and Moore, D. J. P.: Evaluation of a Data Assimilation System for Land Surface Models Using CLM4.5, Journal of Advances in Modeling Earth Systems, 10, 2471–2494, https://doi.org/https://doi.org/10.1029/2018MS001362, 2018.

Frankenberg, C., Fisher, J. B., Worden, J., Badgley, G., Saatchi, S. S., Lee, J.-E., Toon, G. C., Butz, A., Jung, M., Kuze, A., and Yokota, T.: New global observations of the terrestrial carbon cycle from GOSAT: Patterns of plant fluorescence with gross primary productivity, Geophysical Research Letters, 38, https://doi.org/https://doi.org/10.1029/2011GL048738, 2011.

Fratini, G. and Mauder, M.: Towards a consistent eddy-covariance processing: an intercomparison of EddyPro and TK3, Atmospheric Measurement Techniques, 7, 2273–2281, https://doi.org/10.5194/amt-7-2273-2014, 2014.

Frei, M. and Künsch, H. R.: Bridging the ensemble Kalman and particle filters, Biometrika, 100, 781–800, https://doi.org/10.1093/biomet/ast020, 2013.

Friedl, M., McIver, D., Hodges, J., Zhang, X., Muchoney, D., Strahler, A., Woodcock, C., Gopal, S., Schneider, A., Cooper, A., Baccini, A., Gao, F., and Schaaf, C.: Global land cover mapping from MODIS: algorithms and early results, Remote Sensing of Environment, 83, 287–302, https://doi.org/https://doi.org/10.1016/S0034-4257(02)00078-0, the Moderate Resolution Imaging Spectroradiometer (MODIS): a new generation of Land Surface Monitoring, 2002.

Friedlingstein, P., Jones, M. W., O'Sullivan, M., Andrew, R. M., Bakker, D. C. E., Hauck, J., Le Quéré, C., Peters, G. P., Peters, W., Pongratz, J., Sitch, S., Canadell, J. G., Ciais, P., Jackson, R. B., Alin, S. R., Anthoni, P., Bates, N. R., Becker, M., Bellouin, N., Bopp, L., Chau, T. T. T., Chevallier, F., Chini, L. P., Cronin, M., Currie, K. I., Decharme, B., Djeutchouang, L. M., Dou, X., Evans, W., Feely, R. A., Feng, L., Gasser, T., Gilfillan, D., Gkritzalis, T., Grassi, G., Gregor, L., Gruber, N., Gürses, O., Harris, I., Houghton, R. A., Hurtt, G. C., Iida, Y., Ilyina, T., Luijkx, I. T., Jain, A., Jones, S. D., Kato, E., Kennedy, D., Klein Goldewijk, K., Knauer, J., Korsbakken, J. I., Körtzinger, A., Landschützer, P., Lauvset, S. K., Lefèvre, N., Lienert, S., Liu, J., Marland, G., McGuire, P. C., Melton, J. R., Munro, D. R., Nabel, J. E. M. S., Nakaoka, S.-I., Niwa, Y., Ono, T., Pierrot, D., Poulter, B., Rehder, G., Resplandy, L., Robertson, E., Rödenbeck, C., Rosan, T. M., Schwinger, J., Schwingshackl, C., Séférian, R., Sutton, A. J., Sweeney, C., Tanhua, T., Tans, P. P., Tian, H., Tilbrook, B., Tubiello, F., van der Werf, G. R., Vuichard, N., Wada, C., Wanninkhof, R., Watson, A. J., Willis, D., Wiltshire, A. J., Yuan, W., Yue, C., Yue, X., Zaehle, S., and Zeng, J.: Global Carbon Budget 2021, Earth System Science Data, 14, 1917–2005, https://doi.org/10.5194/essd-14-1917-2022, 2022.

Fuchsberger, J., Kirchengast, G., and Kabas, T.: WegenerNet high-resolution weather and climate data from 2007 to 2020, Earth System Science Data, 13, 1307–1334, https://doi.org/10.5194/essd-13-1307-2021, 2021.

Gim, H.-J., Park, S. K., Kang, M., Thakuri, B. M., Kim, J., and Ho, C.-H.: An improved parameterization of the allocation of assimilated carbon to plant parts in vegetation dynamics for Noah-MP, Journal of Advances in Modeling Earth Systems, 9, 1776–1794, https://doi.org/https://doi.org/10.1002/2016MS000890, 2017.

Girotto, M., Reichle, R. H., Rodell, M., Liu, Q., Mahanama, S., and De Lannoy, G. J.: Multi-sensor assimilation of SMOS brightness temperature and GRACE terrestrial water storage observations for soil moisture and shallow groundwater estimation, Remote Sensing of Environment, 227, 12–27, https://doi.org/https://doi.org/10.1016/j.rse.2019.04.001, 2019.

https://doi.org/10.5194/egusphere-2022-1137
Preprint. Discussion started: 20 December 2022

González-Zamora, Á., Sánchez, N., Pablos, M., and Martínez-Fernández, J.: CCI soil moisture assessment with SMOS soil moisture and in situ data under different environmental conditions and spatial scales in Spain, Remote Sensing of Environment, 225, 469–482, https://doi.org/10.1016/j.rse.2018.02.010, 2019.

GRDC: Watershed Boundaries of GRDC Stations, Global Runoff Data Centre. Koblenz, Germany: Federal Institute of Hydrology (BfG), 2011.

Green, J. K., Seneviratne, S. I., Berg, A. M., Findell, K. L., Hagemann, S., Lawrence, D. M., and Gentine, P.: Large influence of soil moisture on long-term terrestrial carbon uptake, Nature, 565, 476–479, 2019.

Gruber, A., Scanlon, T., van der Schalie, R., Wagner, W., and Dorigo, W.: Evolution of the ESA CCI Soil Moisture climate data records and their underlying merging methodology, Earth System Science Data, pp. 1–37, 2019.

Gruber, A., De Lannoy, G., Albergel, C., Al-Yaari, A., Brocca, L., Calvet, J.-C., Colliander, A., Cosh, M., Crow, W., Dorigo, W., Draper, C., Hirschi, M., Kerr, Y., Konings, A., Lahoz, W., McColl, K., Montzka, C., Muñoz-Sabater, J., Peng, J., Reichle, R., Richaume, P., Rüdiger, C., Scanlon, T., van der Schalie, R., Wigneron, J.-P., and Wagner, W.: Validation practices for satellite soil moisture retrievals: What are (the) errors?, Remote Sensing of Environment, 244, 111 806, https://doi.org/https://doi.org/10.1016/j.rse.2020.111806, 2020.

Hansen, M. C., DeFries, R. S., Townshend, J. R., and Sohlberg, R.: Global land cover classification at 1 km spatial resolution using a classification tree approach, International journal of remote sensing, 21, 1331–1364, 2000.

Hashimoto, H., Nemani, R. R., Bala, G., Cao, L., Michaelis, A. R., Ganguly, S., Wang, W., Milesi, C., Eastman, R., Lee, T., et al.: Constraints to vegetation growth reduced by region-specific changes in seasonal climate, Climate, 7, 27, 2019.

Hersbach, H., Bell, B., Berrisford, P., Hirahara, S., Horányi, A., Muñoz-Sabater, J., Nicolas, J., Peubey, C., Radu, R., Schepers, D., Simmons, A., Soci, C., Abdalla, S., Abellan, X., Balsamo, G., Bechtold, P., Biavati, G., Bidlot, J., Bonavita, M., De Chiara, G., Dahlgren, P., Dee, D., Diamantakis, M., Dragani, R., Flemming, J., Forbes, R., Fuentes, M., Geer, A., Haimberger, L., Healy, S., Hogan, R. J., Hólm, E., Janisková, M., Keeley, S., Laloyaux, P., Lopez, P., Lupu, C., Radnoti, G., de Rosnay, P., Rozum, I., Vamborg, F., Villaume, S., and Thépaut, J.-N.: The ERA5 global reanalysis, Quarterly Journal of the Royal Meteorological Society, 146, 1999–2049, https://doi.org/https://doi.org/10.1002/qj.3803, 2020.

Heyvaert, Z., Scherrer, S., Bechtold, M., Gruber, A., Dorigo, W., Kumar, S., and De Lannoy, G.: Impact of design factors for ESA CCI satellite soil moisture data assimilation over Europe, Journal of Hydrometeorology, 2022, in review.

Huang, A., Shen, R., Shi, C., and Sun, S.: Effects of satellite LAI data on modelling land surface temperature and related energy budget in the Noah-MP land surface model, Journal of Hydrology, 613, 128 351, https://doi.org/https://doi.org/10.1016/j.jhydrol.2022.128351, 2022.

Ikonen, J., Vehviläinen, J., Rautiainen, K., Smolander, T., Lemmetyinen, J., Bircher, S., and Pulliainen, J.: The Sodankylä in situ soil moisture observation network: an example application of ESA CCI soil moisture product evaluation, Geoscientific Instrumentation, Methods and Data Systems, 5, 95–108, https://doi.org/10.5194/gi-5-95-2016, 2016.

Ikonen, J., Smolander, T., Rautiainen, K., Cohen, J., Lemmetyinen, J., Salminen, M., and Pulliainen, J.: Spatially distributed evaluation of ESA CCI Soil Moisture products in a northern boreal forest environment, Geosciences, 8, 51, 2018.

Jarlan, L., Balsamo, G., Lafont, S., Beljaars, A., Calvet, J. C., and Mougin, E.: Analysis of leaf area index in the ECMWF land surface model and impact on latent heat and carbon fluxes: Application to West Africa, Journal of Geophysical Research: Atmospheres, 113, https://doi.org/https://doi.org/10.1029/2007JD009370, 2008.

Jensen, K. H. and Refsgaard, J. C.: HOBE: The Danish hydrological observatory, Vadose Zone Journal, 17, 1–24, 2018.

Joiner, J. and Yoshida, Y.: Satellite-based reflectances capture large fraction of variability in global gross primary production (GPP) at weekly time scales, Agricultural and Forest Meteorology, 291, 108 092, https://doi.org/https://doi.org/10.1016/j.agrformet.2020.108092, 2020.

https://doi.org/10.5194/egusphere-2022-1137
Preprint. Discussion started: 20 December 2022

Joiner, J. and Yoshida, Y.: Global MODIS and FLUXNET-derived Daily Gross Primary Production, V2, ORNL DAAC, Oak Ridge, Tennessee, https://doi.org/10.3334/ORNLDAAC/1835, 2021.

Joiner, J., Yoshida, Y., Zhang, Y., Duveiller, G., Jung, M., Lyapustin, A., Wang, Y., and Tucker, C. J.: Estimation of Terrestrial Global Gross Primary Production (GPP) with Satellite Data-Driven Models and Eddy Covariance Flux Data, Remote Sensing, 10, https://doi.org/10.3390/rs10091346, 2018.

Khaki, M., Hendricks Franssen, H.-J., and Han, S.: Multi-mission satellite remote sensing data for improving land hydrological models via data assimilation, Scientific reports, 10, 1–23, 2020.

Kirchengast, G., Kabas, T., Leuprecht, A., Bichler, C., and Truhetz, H.: WegenerNet: A Pioneering High-Resolution Network for Monitoring Weather and Climate, Bulletin of the American Meteorological Society, 95, 227 – 242, https://doi.org/10.1175/BAMS-D-11-00161.1, 2014.

Kolassa, J., Reichle, R. H., Koster, R. D., Liu, Q., Mahanama, S., and Zeng, F.-W.: An Observation-Driven Approach to Improve Vegetation Phenology in a Global Land Surface Model, Journal of Advances in Modeling Earth Systems, 12, e2020MS002 083, https://doi.org/https://doi.org/10.1029/2020MS002083, e2020MS002083 10.1029/2020MS002083, 2020.

Koster, R. D., Walker, G. K., Mahanama, S. P. P., and Reichle, R. H.: Soil Moisture Initialization Error and Subgrid Variability of Precipitation in Seasonal Streamflow Forecasting, Journal of Hydrometeorology, 15, 69 – 88, https://doi.org/10.1175/JHM-D-13-050.1, 2014.

Koster, R. D., Liu, Q., Mahanama, S. P. P., and Reichle, R. H.: Improved Hydrological Simulation Using SMAP Data: Relative Impacts of Model Calibration and Data Assimilation, Journal of Hydrometeorology, 19, 727 – 741, https://doi.org/10.1175/JHM-D-17-0228.1, 2018.

Kumar, S., Peters-Lidard, C., Tian, Y., Houser, P., Geiger, J., Olden, S., Lighty, L., Eastman, J., Doty, B., Dirmeyer, P., Adams, J., Mitchell, K., Wood, E., and Sheffield, J.: Land information system: An interoperable framework for high resolution land surface modeling, Environmental Modelling & Software, 21, 1402–1415, https://doi.org/https://doi.org/10.1016/j.envsoft.2005.07.004, 2006.

Kumar, S. V., Reichle, R. H., Koster, R. D., Crow, W. T., and Peters-Lidard, C. D.: Role of subsurface physics in the assimilation of surface soil moisture observations, Journal of hydrometeorology, 10, 1534–1547, 2009.

Kumar, S. V., Peters-Lidard, C. D., Mocko, D., Reichle, R., Liu, Y., Arsenault, K. R., Xia, Y., Ek, M., Riggs, G., Livneh, B., and Cosh, M.: Assimilation of Remotely Sensed Soil Moisture and Snow Depth Retrievals for Drought Estimation, Journal of Hydrometeorology, 15, 2446 – 2469, https://doi.org/10.1175/JHM-D-13-0132.1, 2014.

Kumar, S. V., Jasinski, M., Mocko, D. M., Rodell, M., Borak, J., Li, B., Beaudoing, H. K., and Peters-Lidard, C. D.: NCA-LDAS Land Analysis: Development and Performance of a Multisensor, Multivariate Land Data Assimilation System for the National Climate Assessment, Journal of Hydrometeorology, 20, 1571 – 1593, https://doi.org/10.1175/JHM-D-17-0125.1, 2019a.

Kumar, S. V., M. Mocko, D., Wang, S., Peters-Lidard, C. D., and Borak, J.: Assimilation of remotely sensed leaf area index into the Noah-MP land surface model: impacts on water and carbon fluxes and states over the continental United States, Journal of Hydrometeorology, 20, 1359–1377, 2019b.

Kumar, S. V., Holmes, T. R., Bindlish, R., de Jeu, R., and Peters-Lidard, C.: Assimilation of vegetation optical depth retrievals from passive microwave radiometry, Hydrology and Earth System Sciences, 24, 3431–3450, https://doi.org/10.5194/hess-24-3431-2020, 2020.

Kumar, S. V., Holmes, T., Andela, N., Dharssi, I., Vinodkumar, Hain, C., Peters-Lidard, C., Mahanama, S. P., Arsenault, K. R., Nie, W., and Getirana, A.: The 2019–2020 Australian Drought and Bushfires Altered the Partitioning of Hydrological Fluxes, Geophysical Research Letters, 48, e2020GL091 411, https://doi.org/https://doi.org/10.1029/2020GL091411, e2020GL091411 2020GL091411, 2021.

Laanaia, N., Carrer, D., Calvet, J.-C., and Pagé, C.: How will climate change affect the vegetation cycle over France? A generic modeling approach, Climate Risk Management, 13, 31–42, https://doi.org/https://doi.org/10.1016/j.crm.2016.06.001, 2016.

Lawrence, D. M., Oleson, K. W., Flanner, M. G., Thornton, P. E., Swenson, S. C., Lawrence, P. J., Zeng, X., Yang, Z.-L., Levis, S., Sakaguchi, K., Bonan, G. B., and Slater, A. G.: Parameterization improvements and functional and structural advances in Version 4 of the Community Land Model, Journal of Advances in Modeling Earth Systems, 3, https://doi.org/https://doi.org/10.1029/2011MS00045, 2011.

Lawrence, D. M., Fisher, R. A., Koven, C. D., Oleson, K. W., Swenson, S. C., Bonan, G., Collier, N., Ghimire, B., van Kampenhout, L., Kennedy, D., Kluzek, E., Lawrence, P. J., Li, F., Li, H., Lombardozzi, D., Riley, W. J., Sacks, W. J., Shi, M., Vertenstein, M., Wieder, W. R., Xu, C., Ali, A. A., Badger, A. M., Bisht, G., van den Broeke, M., Brunke, M. A., Burns, S. P., Buzan, J., Clark, M., Craig, A., Dahlin, K., Drewniak, B., Fisher, J. B., Flanner, M., Fox, A. M., Gentine, P., Hoffman, F., Keppel-Aleks, G., Knox, R., Kumar, S., Lenaerts, J., Leung, L. R., Lipscomb, W. H., Lu, Y., Pandey, A., Pelletier, J. D., Perket, J., Randerson, J. T., Ricciuto, D. M., Sanderson, B. M., Slater, A., Subin, Z. M., Tang, J., Thomas, R. Q., Val Martin, M., and Zeng, X.: The Community Land Model Version 5: Description of New Features, Benchmarking, and Impact of Forcing Uncertainty, Journal of Advances in Modeling Earth Systems, 11, 4245–4287, https://doi.org/https://doi.org/10.1029/2018MS001583, 2019.

Leroux, D. J., Calvet, J.-C., Munier, S., and Albergel, C.: Using satellite-derived vegetation products to evaluate LDAS-Monde over the Euro-Mediterranean area, Remote Sensing, 10, 1199, 2018.

Li, J., Miao, C., Zhang, G., Fang, Y.-H., Shangguan, W., and Niu, G.-Y.: Global Evaluation of the Noah-MP Land Surface Model and Suggestions for Selecting Parameterization Schemes, Journal of Geophysical Research: Atmospheres, 127, e2021JD035 753, https://doi.org/https://doi.org/10.1029/2021JD035753, e2021JD035753 2021JD035753, 2022.

Lievens, H., Martens, B., Verhoest, N., Hahn, S., Reichle, R., and Miralles, D.: Assimilation of global radar backscatter and radiometer brightness temperature observations to improve soil moisture and land evaporation estimates, Remote Sensing of Environment, 189, 194–210, https://doi.org/https://doi.org/10.1016/j.rse.2016.11.022, 2017.

Ling, X. L., Fu, C. B., Guo, W. D., and Yang, Z.-L.: Assimilation of Remotely Sensed LAI Into CLM4CN Using DART, Journal of Advances in Modeling Earth Systems, 11, 2768–2786, https://doi.org/https://doi.org/10.1029/2019MS001634, 2019.

Loew, A., Dall'Amico, J. T., Schlenz, F., and Mauser, W.: The Upper Danube Soil Moisture Validation Site: Measurements and Activities, in: Earth Observation and Water Cycle Science, edited by Lacoste, H., vol. 674 of *ESA Special Publication*, p. 56, 2009.

Ma, N., Niu, G.-Y., Xia, Y., Cai, X., Zhang, Y., Ma, Y., and Fang, Y.: A Systematic Evaluation of Noah-MP in Simulating Land-Atmosphere Energy, Water, and Carbon Exchanges Over the Continental United States, Journal of Geophysical Research: Atmospheres, 122, 12,245–12,268, https://doi.org/https://doi.org/10.1002/2017JD027597, 2017.

MacBean, N., Maignan, F., Peylin, P., Bacour, C., Bréon, F.-M., and Ciais, P.: Using satellite data to improve the leaf phenology of a global terrestrial biosphere model, Biogeosciences, 12, 7185–7208, https://doi.org/10.5194/bg-12-7185-2015, 2015.

MacBean, N., Peylin, P., Chevallier, F., Scholze, M., and Schürmann, G.: Consistent assimilation of multiple data streams in a carbon cycle data assimilation system, Geoscientific Model Development, 9, 3569–3588, https://doi.org/10.5194/gmd-9-3569-2016, 2016.

Maertens, M., De Lannoy, G. J. M., Apers, S., Kumar, S. V., and Mahanama, S. P. P.: Land surface modeling over the Dry Chaco: the impact of model structures, and soil, vegetation and land cover parameters, Hydrology and Earth System Sciences, 25, 4099–4125, https://doi.org/10.5194/hess-25-4099-2021, 2021.

Maes, W. H., Pagán, B. R., Martens, B., Gentine, P., Guanter, L., Steppe, K., Verhoest, N. E., Dorigo, W., Li, X., Xiao, J., and Miralles, D. G.: Sun-induced fluorescence closely linked to ecosystem transpiration as evidenced by satellite data and radiative transfer models, Remote Sensing of Environment, 249, 112 030, https://doi.org/https://doi.org/10.1016/j.rse.2020.112030, 2020.

Mahmud, K., Scott, R. L., Biederman, J. A., Litvak, M. E., Kolb, T., Meyers, T. P., Krishnan, P., Bastrikov, V., and MacBean, N.: Optimizing Carbon Cycle Parameters Drastically Improves Terrestrial Biosphere Model Underestimates of Dryland Mean Net CO2 Flux and its

https://doi.org/10.5194/egusphere-2022-1137
Preprint. Discussion started: 20 December 2022

Inter-Annual Variability, Journal of Geophysical Research: Biogeosciences, 126, https://doi.org/https://doi.org/10.1029/2021JG006400, 2021.

Marczewski, W., Slominski, J., Slominska, E., Usowicz, B., Usowicz, J., S, R., O, M., Nastula, J., and Zawadzki, J.: Strategies for validating and directions for employing SMOS data, in the Cal-Val project SWEX (3275) for wetlands, Hydrology and Earth System Sciences Discussions, 7, https://doi.org/10.5194/hessd-7-7007-2010, 2010.

Martens, B., Miralles, D. G., Lievens, H., van der Schalie, R., de Jeu, R. A. M., Fernández-Prieto, D., Beck, H. E., Dorigo, W. A., and Verhoest, N. E. C.: GLEAM v3: satellite-based land evaporation and root-zone soil moisture, Geoscientific Model Development, 10, 1903–1925, https://doi.org/10.5194/gmd-10-1903-2017, 2017.

Miralles, D. G., Holmes, T. R. H., De Jeu, R. A. M., Gash, J. H., Meesters, A. G. C. A., and Dolman, A. J.: Global land-surface evaporation estimated from satellite-based observations, Hydrology and Earth System Sciences, 15, 453–469, https://doi.org/10.5194/hess-15-453-2011, 2011.

Miralles, D. G., Nieto, R., McDowell, N. G., Dorigo, W. A., Verhoest, N. E., Liu, Y. Y., Teuling, A. J., Dolman, A. J., Good, S. P., and Gimeno, L.: Contribution of water-limited ecoregions to their own supply of rainfall, Environmental Research Letters, 11, 124 007, https://doi.org/10.1088/1748-9326/11/12/124007, 2016.

Mitchell, H. L., Houtekamer, P. L., and Pellerin, G.: Ensemble Size, Balance, and Model-Error Representation in an Ensemble Kalman Filter, Monthly Weather Review, 130, 2791 – 2808, https://doi.org/10.1175/1520-0493(2002)130<2791:ESBAME>2.0.CO;2, 2002.

Mocko, D. M., Kumar, S. V., Peters-Lidard, C. D., and Wang, S.: Assimilation of Vegetation Conditions Improves the Representation of Drought over Agricultural Areas, Journal of Hydrometeorology, 22, 1085 – 1098, https://doi.org/10.1175/JHM-D-20-0065.1, 2021.

Morbidelli, R., Saltalippi, C., Flammini, A., Cifrodelli, M., Picciafuoco, T., Corradini, C., and Govindaraju, R. S.: In situ measurements of soil saturated hydraulic conductivity: Assessment of reliability through rainfall–runoff experiments, Hydrological Processes, 31, 3084–3094, 2017.

Mucia, A., Bonan, B., Zheng, Y., Albergel, C., and Calvet, J.-C.: From Monitoring to Forecasting Land Surface Conditions Using a Land Data Assimilation System: Application over the Contiguous United States, Remote Sensing, 12, 2020.

Mucia, A., Bonan, B., Albergel, C., Zheng, Y., and Calvet, J.-C.: Assimilation of passive microwave vegetation optical depth in LDAS-Monde: a case study over the continental US, Biogeosciences Discussions, 2021, 1–45, https://doi.org/10.5194/bg-2021-248, 2021.

Naeimi, V., Scipal, K., Bartalis, Z., Hasenauer, S., and Wagner, W.: An improved soil moisture retrieval algorithm for ERS and METOP scatterometer observations, IEEE Transactions on Geoscience and Remote Sensing, 47, 1999–2013, 2009.

Nair, R. K. F., Morris, K. A., Hertel, M., Luo, Y., Moreno, G., Reichstein, M., Schrumpf, M., and Migliavacca, M.: N : P stoichiometry and habitat effects on Mediterranean savanna seasonal root dynamics, Biogeosciences, 16, 1883–1901, https://doi.org/10.5194/bg-16-1883-2019, 2019.

Nie, W., Kumar, S. V., Arsenault, K. R., Peters-Lidard, C. D., Mladenova, I. E., Bergaoui, K., Hazra, A., Zaitchik, B. F., Mahanama, S. P., McDonnell, R., Mocko, D. M., and Navari, M.: Towards effective drought monitoring in the Middle East and North Africa (MENA) region: implications from assimilating leaf area index and soil moisture into the Noah-MP land surface model for Morocco, Hydrology and Earth System Sciences, 26, 2365–2386, https://doi.org/10.5194/hess-26-2365-2022, 2022.

Niu, G.-Y., Yang, Z.-L., Mitchell, K. E., Chen, F., Ek, M. B., Barlage, M., Kumar, A., Manning, K., Niyogi, D., Rosero, E., Tewari, M., and Xia, Y.: The community Noah land surface model with multiparameterization options (Noah-MP): 1. Model description and evaluation with local-scale measurements, Journal of Geophysical Research: Atmospheres, 116, https://doi.org/https://doi.org/10.1029/2010JD015139, 2011.

Niu, G.-Y., Fang, Y.-H., Chang, L.-L., Jin, J., Yuan, H., and Zeng, X.: Enhancing the Noah-MP Ecosystem Response to Droughts With an Explicit Representation of Plant Water Storage Supplied by Dynamic Root Water Uptake, Journal of Advances in Modeling Earth Systems, 12, e2020MS002 062, https://doi.org/https://doi.org/10.1029/2020MS002062, e2020MS002062 2020MS002062, 2020.

Owe, M., de Jeu, R., and Holmes, T.: Multisensor historical climatology of satellite-derived global land surface moisture, Journal of Geophysical Research: Earth Surface, 113, 2008.

Parrens, M., Mahfouf, J.-F., Barbu, A. L., and Calvet, J.-C.: Assimilation of surface soil moisture into a multilayer soil model: design and evaluation at local scale, Hydrology and Earth System Sciences, 18, 673–689, https://doi.org/10.5194/hess-18-673-2014, 2014.

Paulik, C., Preimesberger, W., Scherrer, S., Stradiotti, P., Hahn, S., Baum, D., Plocon, A., Mistelbauer, T., Scanlon, T., Schmitzer, M., Gruber, A., Teubner, I., and teije01, .: pytesmo - a Python Toolbox for the Evaluation of Soil Moisture observations, https://doi.org/https://doi.org/10.5281/zenodo.596422, 2022.

Peters-Lidard, C. D., Houser, P. R., Tian, Y., Kumar, S. V., Geiger, J., Olden, S., Lighty, L., Doty, B., Dirmeyer, P., Adams, J., et al.: High-performance Earth system modeling with NASA/GSFC's Land Information System, Innovations in Systems and Software Engineering, 3, 157–165, 2007.

Petropoulos, G. P. and McCalmont, J. P.: An operational in situ soil moisture & soil temperature monitoring network for West Wales, UK: The WSMN network, Sensors, 17, 1481, https://doi.org/10.3390/s17071481, 2017.

Preimesberger, W., Scanlon, T., Su, C., Gruber, A., and Dorigo, W.: Homogenization of Structural Breaks in the Global ESA CCI Soil Moisture Multisatellite Climate Data Record, IEEE Transactions on Geoscience and Remote Sensing, pp. 1–18, https://doi.org/10.1109/TGRS.2020.3012896, 2020.

Raffelli, G., Previati, M., Canone, D., Gisolo, D., Bevilacqua, I., Capello, G., Biddoccu, M., Cavallo, E., Deiana, R., Cassiani, G., et al.: Local-and plot-scale measurements of soil moisture: Time and spatially resolved field techniques in plain, hill and mountain sites, Water, 9, 706, 2017.

Rahman, A., Zhang, X., Houser, P., Sauer, T., and Maggioni, V.: Global Assimilation of Remotely Sensed Leaf Area Index: The Impact of Updating More State Variables Within a Land Surface Model, Frontiers in Water, 3, https://doi.org/10.3389/frwa.2021.789352, 2022.

Reichle, R. H. and Koster, R. D.: Bias reduction in short records of satellite soil moisture, Geophysical Research Letters, 31, https://doi.org/https://doi.org/10.1029/2004GL020938, 2004.

Rodell, M., Houser, P. R., Jambor, U., Gottschalck, J., Mitchell, K., Meng, C.-J., Arsenault, K., Cosgrove, B., Radakovich, J., Bosilovich, M., Entin, J. K., Walker, J. P., Lohmann, D., and Toll, D.: The Global Land Data Assimilation System, Bulletin of the American Meteorological Society, 85, 381 – 394, https://doi.org/10.1175/BAMS-85-3-381, 2004.

Ryu, D., Crow, W. T., Zhan, X., and Jackson, T. J.: Correcting Unintended Perturbation Biases in Hydrologic Data Assimilation, Journal of Hydrometeorology, 10, 734 – 750, https://doi.org/10.1175/2008JHM1038.1, 2009.

Sabater, J. M., Rüdiger, C., Calvet, J.-C., Fritz, N., Jarlan, L., and Kerr, Y.: Joint assimilation of surface soil moisture and LAI observations into a land surface model, Agricultural and Forest Meteorology, 148, 1362–1373, https://doi.org/https://doi.org/10.1016/j.agrformet.2008.04.003, 2008.

Sawada, Y. and Koike, T.: Simultaneous estimation of both hydrological and ecological parameters in an ecohydrological model by assimilating microwave signal, Journal of Geophysical Research: Atmospheres, 119, 8839–8857, https://doi.org/https://doi.org/10.1002/2014JD021536, 2014.

Sawada, Y., Koike, T., and Walker, J. P.: A land data assimilation system for simultaneous simulation of soil moisture and vegetation dynamics, Journal of Geophysical Research: Atmospheres, 120, 5910–5930, https://doi.org/https://doi.org/10.1002/2014JD022895, 2015.

Schlenz, F., dall'Amico, J. T., Loew, A., and Mauser, W.: Uncertainty Assessment of the SMOS Validation in the Upper Danube Catchment, IEEE Transactions on Geoscience and Remote Sensing, 50, 1517–1529, 2012.

Scholze, M., Kaminski, T., Knorr, W., Voßbeck, M., Wu, M., Ferrazzoli, P., Kerr, Y., Mialon, A., Richaume, P., Rodríguez-Fernández, N., Vittucci, C., Wigneron, J.-P., Mecklenburg, S., and Drusch, M.: Mean European Carbon Sink Over 2010–2015 Estimated by Simultaneous Assimilation of Atmospheric CO2, Soil Moisture, and Vegetation Optical Depth, Geophysical Research Letters, 46, 13 796–13 803, https://doi.org/https://doi.org/10.1029/2019GL085725, 2019.

Skamarock, W. C., Klemp, J. B., Dudhia, J., Gill, D. O., Liu, Z., Berner, J., Wang, W., Powers, J. G., Duda, M. G., Barker, D. M., et al.: A description of the advanced research WRF model version 4, National Center for Atmospheric Research: Boulder, CO, USA, 145, 145, 2019.

Smets, B., Verger, A., Camacho, F., der Goten, R. V., and Jacobs, T.: Copernicus Global Land Operations "Vegetation and Energy" – Product User Manual – LAI/FAPAR/FCover, Collection 1km, Version 2, Tech. rep., Copernicus, 2019.

Tharammal, T., Bala, G., Devaraju, N., and Nemani, R.: A review of the major drivers of the terrestrial carbon uptake: model-based assessments, consensus, and uncertainties, Environmental Research Letters, 14, 093 005, https://doi.org/10.1088/1748-9326/ab3012, 2019a.

Tharammal, T., Bala, G., Narayanappa, D., and Nemani, R.: Potential roles of CO2 fertilization, nitrogen deposition, climate change, and land use and land cover change on the global terrestrial carbon uptake in the twenty-first century, Climate Dynamics, 52, 4393–4406, 2019b.

Tian, Y., Peters-Lidard, C. D., Kumar, S. V., Geiger, J., Houser, P. R., Eastman, J. L., Dirmeyer, P., Doty, B., and Adams, J.: High-performance land surface modeling with a Linux cluster, Computers & Geosciences, 34, 1492–1504, 2008.

van Leeuwen, P. J., Künsch, H. R., Nerger, L., Potthast, R., and Reich, S.: Particle filters for high-dimensional geoscience applications: A review, Quarterly Journal of the Royal Meteorological Society, 145, 2335–2365, https://doi.org/https://doi.org/10.1002/qj.3551, 2019.

Verger, A., Baret, F., and Weiss, M.: Near Real-Time Vegetation Monitoring at Global Scale, IEEE Journal of Selected Topics in Applied Earth Observations and Remote Sensing, 7, 3473–3481, https://doi.org/10.1109/JSTARS.2014.2328632, 2014.

Vreugdenhil, M., Dorigo, W., Broer, M., Haas, P., Eder, A., Hogan, P., Blöschl, G., and Wagner, W.: Towards a high-density soil moisture network for the validation of SMAP in Petzenkirchen, Austria, in: 2013 IEEE International Geoscience and Remote Sensing Symposium-IGARSS, pp. 1865–1868, IEEE, 2013.

Wagner, W., Lemoine, G., and Rott, H.: A Method for Estimating Soil Moisture from ERS Scatterometer and Soil Data, Remote Sensing of Environment, 70, 191–207, https://doi.org/https://doi.org/10.1016/S0034-4257(99)00036-X, 1999.

Walker, A. P., De Kauwe, M. G., Bastos, A., Belmecheri, S., Georgiou, K., Keeling, R. F., McMahon, S. M., Medlyn, B. E., Moore, D. J. P., Norby, R. J., Zaehle, S., Anderson-Teixeira, K. J., Battipaglia, G., Brienen, R. J. W., Cabugao, K. G., Cailleret, M., Campbell, E., Canadell, J. G., Ciais, P., Craig, M. E., Ellsworth, D. S., Farquhar, G. D., Fatichi, S., Fisher, J. B., Frank, D. C., Graven, H., Gu, L., Haverd, V., Heilman, K., Heimann, M., Hungate, B. A., Iversen, C. M., Joos, F., Jiang, M., Keenan, T. F., Knauer, J., Körner, C., Leshyk, V. O., Leuzinger, S., Liu, Y., MacBean, N., Malhi, Y., McVicar, T. R., Penuelas, J., Pongratz, J., Powell, A. S., Riutta, T., Sabot, M. E. B., Schleucher, J., Sitch, S., Smith, W. K., Sulman, B., Taylor, B., Terrer, C., Torn, M. S., Treseder, K. K., Trugman, A. T., Trumbore, S. E., van Mantgem, P. J., Voelker, S. L., Whelan, M. E., and Zuidema, P. A.: Integrating the evidence for a terrestrial carbon sink caused by increasing atmospheric CO2, New Phytologist, 229, 2413–2445, https://doi.org/https://doi.org/10.1111/nph.16866, 2021.

Wen, J., Koehler, P., Duveiller, G., Parazoo, N., Magney, T., Hooker, G., Yu, L., Chang, C., and Sun, Y.: Global High-Resolution Estimates of SIF from Fused SCIAMACHY and GOME-2, 2002-2018, ORNL DAAC, Oak Ridge, Tennessee, https://doi.org/10.3334/ORNLDAAC/1864, 2021.

https://doi.org/10.5194/egusphere-2022-1137
Preprint. Discussion started: 20 December 2022

Wigneron, J.-P., Dayan, S., Kruszewski, A., Aluome, C., AI-Yaari, M. G.-E. A., Fan, L., Guven, S., Chipeaux, C., Moisy, C., Guyon, D., et al.: The aqui network: soil moisture sites in the “Les landes” forest and graves vineyards (Bordeaux aquitaine region, France), in: IGARSS 2018-2018 IEEE International Geoscience and Remote Sensing Symposium, pp. 3739–3742, IEEE, 2018.

Wutzler, T., Lucas-Moffat, A., Migliavacca, M., Knauer, J., Sickel, K., Šigut, L., Menzer, O., and Reichstein, M.: Basic and extensible post-processing of eddy covariance flux data with REddyProc, Biogeosciences, 15, 5015–5030, https://doi.org/10.5194/bg-15-5015-2018, 2018.

Xu, T., Chen, F., He, X., Barlage, M., Zhang, Z., Liu, S., and He, X.: Improve the Performance of the Noah-MP-Crop Model by Jointly Assimilating Soil Moisture and Vegetation Phenology Data, Journal of Advances in Modeling Earth Systems, 13, e2020MS002 394, https://doi.org/https://doi.org/10.1029/2020MS002394, e2020MS002394 2020MS002394, 2021.

Yang, Z.-L., Niu, G.-Y., Mitchell, K. E., Chen, F., Ek, M. B., Barlage, M., Longuevergne, L., Manning, K., Niyogi, D., Tewari, M., and Xia, Y.: The community Noah land surface model with multiparameterization options (Noah-MP): 2. Evaluation over global river basins, Journal of Geophysical Research: Atmospheres, 116, https://doi.org/https://doi.org/10.1029/2010JD015140, 2011.

Yilmaz, M. T. and Crow, W. T.: The Optimality of Potential Rescaling Approaches in Land Data Assimilation, Journal of Hydrometeorology, 14, 650 – 660, https://doi.org/10.1175/JHM-D-12-052.1, 2013.

Zacharias, S., Bogena, H., Samaniego, L., Mauder, M., Fuß, R., Pütz, T., Frenzel, M., Schwank, M., Baessler, C., Butterbach-Bahl, K., Bens, O., Borg, E., Brauer, A., Dietrich, P., Hajnsek, I., Helle, G., Kiese, R., Kunstmann, H., Klotz, S., and Vereecken, H.: A Network of Terrestrial Environmental Observatories in Germany, Vadose Zone Journal, 10, 955–973, https://doi.org/10.2136/vzj2010.0139, 2011.

Zreda, M., Desilets, D., Ferré, T., and Scott, R.: Measuring soil moisture content non-invasively at intermediate spatial scale using cosmic-ray neutrons, Geophysical Research Letters, 35, https://doi.org/10.1029/2008GL035655, 2008.

Zreda, M., Shuttleworth, W. J., Zeng, X., Zweck, C., Desilets, D., Franz, T., and Rosolem, R.: COSMOS: the COsmic-ray Soil Moisture Observing System, Hydrology and Earth System Sciences, 16, 4079–4099, https://doi.org/10.5194/hess-16-4079-2012, 2012.